Acceleration of warming, deoxygenation and acidification in the Arabian Gulf driven by weakening of summer winds

ZOUHAIR LACHKAR[1], Michael Mehari[2], Francesco Francesco Paparella[3], and John A Burt[1]

[1]New York University Abu Dhabi
[2]National Aeronautics and Space Administration, Goddard Space Flight Center
[3]New York University, Abu Dhabi Campus

April 25, 2024

Abstract

The Arabian Gulf (AG) exports hypersaline, dense waters into the Sea of Oman (SOO), replaced by fresher inflowing surface waters from the Indian Ocean. We investigate the impact of recent AG warming on its exchange with the SOO and the implications this has on the AG biogeochemistry. Using an eddy-resolving hindcast model simulation, we analyze the hydrography and biogeochemistry of the AG and the SOO from 1980 to 2018. Our study reveals that changes in summer surface winds have accelerated AG warming and weakened it in the SOO, reducing the density gradient and water exchange between the two seas during late summer. This has led to nutrient buildup, increased productivity, and heightened deoxygenation and acidification in the AG. These findings underscore how subtle wind changes can exacerbate the vulnerability of marginal seas to climate change and stress the need to properly represent regional winds in global climate models.

Abstract

The Arabian Gulf (AG) exports hypersaline, dense waters into the Sea of Oman (SOO), replaced by fresher inflowing surface waters from the Indian Ocean. We investigate the impact of recent AG warming on its exchange with the SOO and the implications this has on the AG biogeochemistry. Using an eddy-resolving hindcast model simulation, we analyze the hydrography and biogeochemistry of the AG and the SOO from 1980 to 2018. Our study reveals that changes in summer surface winds have accelerated AG warming and weakened it in the SOO, reducing the density gradient and water exchange between the two seas during late summer. This has led to nutrient buildup, increased productivity, and heightened deoxygenation and acidification in the AG. These findings underscore how subtle wind changes can exacerbate the vulnerability of marginal seas to climate change and stress the need to properly represent regional winds in global climate models.

Plain Language Summary

The Arabian Gulf (also known as Persian Gulf) produces dense, salty water that flows into the Sea of Oman, while it receives fresher water from the Indian Ocean. This study investigates how the recent rapid warming of the Arabian Gulf affects this exchange with the Sea of Oman and its impact on the Gulf's environment. Using a computer simulation to model the Arabian Gulf's evolution from 1980 to 2018, we discovered that changes in surface winds have warmed the Arabian Gulf and weakened its connection to the Sea of Oman during summer. This led to nutrient accumulation, increased micro-algae growth, decreased oxygen levels, and increased water acidity in the Arabian Gulf. These findings highlight how minor changes in wind patterns can exacerbate the effects of climate change in specific seas, emphasizing the need to improve the representation of local winds in climate models.

1 Introduction

The Arabian Gulf, also known as the Persian Gulf (hereafter AG), is a shallow semi-enclosed sea subject to a hyper-arid climate, characterized by intense evaporation that far exceeds both precipitation and runoff (Reynolds, 1993). This results in the prevalence of large areas of hypersaline waters (Vaughan et al., 2019) and an inverse estuary circulation, in which the dense Gulf water (Gulf Deep Water) is discharged at depth along the southern side of the Strait of Hormuz (hereafter the Strait) into the Sea of Oman (hereafter SOO), and is replaced by a surface inflow of fresher, lower-density waters from the Indian Ocean (Indian Ocean Surface Water) along the northern side of the Strait (Chao et al., 1992; Reynolds, 1993; Swift & Bower, 2003). As direct observations of this exchange and its variability are scarce (Johns et al., 2003; Swift & Bower, 2003), numerous modeling studies have explored its dynamics, revealing its tight coupling to the density gradient through the Strait (Kämpf & Sadrinasab, 2006; Thoppil & Hogan, 2009; Yao & Johns, 2010; Pous et al., 2015; Lorenz et al., 2020). The recent rapid warming of the AG relative to the Arabian Sea (Al-Rashidi et al., 2009; Strong et al., 2011; Hereher, 2020; Al Senafi, 2022), which is expected to further accelerate in the future, is likely to impact the density gradient between the two seas and hence alter transport through the Strait (Swift & Bower, 2003; Kämpf & Sadrinasab, 2006; Paparella et al., 2022). Yet, little is known about the effects of such changes on the AG environment.

The AG is generally considered oligotrophic throughout most of the year because the new waters entering the Gulf mainly flow in at or near the surface, and thus are generally depleted in nutrients, except during winter when convective mixing in the northern Arabian Sea brings nutrients to the surface, triggering a winter bloom that enriches the Gulf source waters in nutrients and organic matter, fertilizing the Gulf in late winter (Al-Yamani & Naqvi, 2019). Consequently, the Gulf has been assumed to be relatively well oxygenated in its pristine state (Al-Yamani & Naqvi, 2019). Moreover, given its high levels of alkalinity, the Gulf is believed to have a high buffering capacity against ocean acidification, a process that can threaten the growth and maintenance of marine calcifiers, including coral reef calcifying organisms (Purkis et al., 2011; Izumi et al., 2022). Yet, recent observations challenge these assumptions. First, observational and modeling evidence suggests that summer near-bottom hypoxia has become regular, more intense, and widespread over recent decades (Al-Ansari et al., 2015; Saleh et al., 2021; Lachkar et al., 2022). Second, observations indicating rapid progression of ocean acidification in the AG have been reported (Uddin et al., 2012). The concomitant occurrence of ocean deoxygenation and ocean acidification may further exacerbate the vulnerability of the AG ecosystems, including its coral reefs, to ongoing warming (Burt et al., 2019; de Verneil et al., 2021; Purkis et al., 2011; Burt & Paparella, 2023).

The drivers behind these biogeochemical changes and the eventual role of the rapid warming of the AG in their emergence remain poorly understood. In particular, the role et al., 2016). Atmospheric pCO_2 data is obtained from Mauna Loa (Keeling et al., 2005) and (Joos & Spahni, 2008). The model is spun-up for 69 years, after which two simulations are conducted: a control hindcast run (HR) forced with increasing atmospheric carbon and interannually varying momentum, freshwater, and heat fluxes from 1980 to 2018, and a constant climate (CC) simulation forced with climatological forcing (repeated normal year) and increasing CO_2. The CC simulation serves to quantify model drift and disentangle the roles of climate change and rising atmospheric CO_2 levels in reported acidification. Our analysis reveals a negligible model drift in the study area. Further details of the model setup and the evaluation of model drift are provided in the SI (Text S2, SI).

We evaluate the model's performance in reproducing key aspects of the region's hydrography and biogeochemistry using the limited available data (Figs S5-S7, SI). Overall, we find that despite some local discrepancies, our model generally captures the essential hydrographic features of the Gulf region, including the seasonal progression of temperature, salinity, and the Gulf outflow. Similarly, our model also aligns relatively well with available data regarding oxygen levels, vertical distribution of chlorophyll, seasonal variability in biological production, as well as the state of the carbonate system (DIC, TA, pCO_2, and pH). A detailed description of the model evaluation is provided in the SI (Text S3, Figs S1-S7).

3 Results

3.1 Seasonal and interannual variability in the AG and the SOO

To put the long-term trends in the AG in broader context, we first characterize the seasonal and interannual variability of both the physical and biogeochemical properties within the AG and the SOO. The temperature in both the AG and the SOO exhibits much stronger seasonal variability than salinity (Figs 1A-1C). Consequently, the seasonal cycle in density in both seas appears to be primarily driven by temperature fluctuations throughout the year rather than variations in salinity. While both the AG and the SOO display strong seasonal variability in temperature, the amplitude of this variability is notably stronger in the AG compared to the SOO. This leads to the amplitude of the variability in surface density being nearly twice as large in the AG relative to the SOO (Fig 1E). Furthermore, the Gulf exhibits significantly higher variability on interannual timescales vis-a-vis the SOO, with a standard deviation 3 to 4 times larger for winter temperature and 5 to 10 times larger for salinity throughout the year (Figs 1A & 1C). These differences are also reflected in surface density, which displays stronger interannual variability in the AG relative to the SOO, with a standard deviation 3 to 4 times larger in the former (Fig 1E).

The strong variability in AG water density results in notable seasonal changes in the density gradient between the AG and the SOO, with the density contrast between the two seas peaking in winter and reaching its lowest point in summer (Fig 1G). The density gradient across the Strait is the primary driver of the overturning circulation, which transports light surface waters from the SOO into the Gulf and dense, deep Gulf waters into the SOO (Swift & Bower, 2003). Consequently, fluctuations in this gradient are expected to cause fluctuations in the strength of the Gulf water outflow (e.g., Swift & Bower, 2003; Kämpf & Sadrinasab, 2006; Paparella et al., 2022). Our analysis of the Gulf outflow at the Strait indeed reveals seasonal variability similar to that of the density gradient, albeit with a time lag of 2 to 3 months (Fig 1G). Maximum outflow occurs in spring, while minimum outflow is observed in late summer and early autumn (Fig 1G). This finding aligns with evidence from previous observational and modeling studies that have investigated the seasonal variability in Gulf outflow (e.g., Johns et al., 2003; Kämpf & Sadrinasab, 2006; Lorenz et al., 2020).

The pronounced variability in hydrography is accompanied by similarly strong seasonality in biogeochemistry in both the AG and the SOO (Figs 1B-1H). Despite faster photosynthetic growth rates in summer driven by higher temperatures, the stronger winter vertical mixing and the net inflow of nutrients from the SOO result in greater biological production in the Gulf during winter than in summer (Figs 1B-1H). Similarly, in the SOO, biological production is higher in winter due to increased nutrient supply from depth because of winter convective mixing in the northern Arabian Sea (Naqvi et al., 2002). Finally, both dissolved oxygen and pH exhibit strong seasonality at depth in both seas, with maximum values occurring in late winter and minimum values in late summer when oxygen deficit and carbon excess driven by respiration accumulate at depth due to limited vertical mixing (Figs 1D-1F).

3.2 Contrasting rates of warming in the AG and the SOO

We model a rapid warming trend in both the AG and the SOO, consistent with observations (Fig 2). While much of the northern Arabian Sea has experienced warming in recent decades, the rate of warming in the AG is nearly 50% faster than in the rest of the Arabian Sea (Fig 2B). During winter, the warming in the AG is not statistically significant and is comparable in magnitude to that of the SOO (Figs 2C-2D). However, during summer the warming in the Gulf is statistically significant and up to three times faster than that observed in the SOO (Figs 2C-2D).

A more comprehensive analysis of long-term trends throughout the year reveals uneven warming patterns in both the AG and the SOO (Fig 3A). Warming is more pronounced in spring and summer and is weakest in winter in the AG. In contrast, warming peaks in spring and fall and is weakest in early summer in the SOO, due to the influence of upwelling along the coast of Oman. In addition to average temperatures, temperature extremes have also been affected by warming in the AG and SOO. Yet, important shifts towards higher extreme temperatures are observed only in summer in the AG and in winter in the SOO (Fig S8, SI). Consequently, temperature emerges from the 1980s historical variability (i.e., exceeding 2 standard deviations above the 1980s climatological means) in summer in the AG and in winter in the SOO (Fig S9, SI) Due to these disparities, along with variations in surface salinity trends between the two seas, the density gradient at the Strait also changes unevenly throughout the year (Fig 3A). Specifically, over the study period, the density contrast slightly increases in early winter but significantly decreases during summer. Consequently, the Gulf outflow strengthens slightly (+3% per decade) in winter but weakens more importantly (up to -10% per decade) in late summer and early autumn (Fig 3A).

3.3 Rapid changes in the biogeochemistry of the AG

Changes in the biogeochemical properties of the AG also display significant variations among the seasons (Fig 3B). For example, nitrogen supply to the Gulf shows a notable increase in early winter (December), coinciding with a significant intensification of water exchange (Fig 3B). However, nitrogen supply to the Gulf also experiences a significant increase during late summer and early autumn (September to October) despite a weakening of the Gulf inflow/outflow driven by warming (Fig 3B). To comprehend this apparent paradox, one must consider not only the strength of the overturning but also the vertical gradient of nutrients at the Strait (Fig S10, SI). In contrast to winter, strong summer stratification induces a pronounced vertical gradient in nitrogen at the Strait, with very low concentrations near the surface and significantly higher levels below 20 m. Consequently, the net nitrogen flux associated with the overturning circulation in summer results in a loss for the AG (outflow waters have a higher nitrogen content than inflow water). Conversely, in winter, surface inflow waters have a higher nitrogen content compared to outflowing waters (Fig S10, SI), leading to a net supply of nitrogen to the Gulf (Fig 3B). Consequently, the significant decrease in outflow during late summer, as well as the increase in early winter, both contribute to an increase in the supply of nitrogen to the Gulf. This buildup of nutrients and biomass in the AG, combined with faster photosynthetic growth rates driven by higher temperatures, leads to enhanced biological production throughout most of the year (Fig 3B). The increase in productivity enhances respiration, particularly in the benthos, resulting in increased consumption of oxygen and the release of carbon dioxide at depth near the seafloor (Fig S11, SI). As the stratification increases in summer, the supply (release) of O_2 (CO_2) from (to) the surface diminishes, causing depletion (accumulation) of O_2 (CO_2), and thus an expansion of hypoxia and low-pH waters near the bottom. This increased acidification, driven by enhanced respiration, compounds the background acidification caused by rising atmospheric CO_2 levels (constant climate), amplifying it by up to 50% in late summer (Fig 3B).

3.4 Drivers of the rapid warming of the AG

An examination of the heat budget in the AG throughout the study period indicates that most of the simulated temperature changes are driven by alterations in atmospheric fluxes, while the lateral transport of heat to and from the SOO has a minor impact (Fig 4A). To understand the processes behind changes in atmospheric forcing, we analyze changes in the individual components of the atmospheric heat fluxes (Figs 4B-4D). Positive statistically significant trends in both incoming radiation and latent heat fluxes contribute to the summer warming in the AG, while changes in sensible heat fluxes play a negligible role. Changes in downward radiation, primarily associated with longwave radiation, contribute to summer warming in both seas (Fig 4B). In contrast, changes in latent heat fluxes amplify warming in most of the AG but dampen it in the SOO (Fig

4C), thus explaining much of the differential warming between the two seas. It's important to note that the contribution of latent heat fluxes to the warming of the Gulf varies spatially and temporally due to high interannual variability. This is consistent with previous works that found that interannual fluctuations in total heat fluxes over the Gulf are dominated by fluctuations in the latent heat fluxes (e.g., Pous et al., 2015; Paparella et al., 2019). Generally, the contribution of latent heat fluxes is more pronounced in the central Gulf and during late summer (August) (Fig S12, SI). In winter, evaporative cooling decreases in both the AG and the SOO, contributing to warming trends in both seas (Fig S12, SI). These long-term trends in latent heat fluxes are primarily driven by changes in surface wind speed in the region (Fig 2E and Fig 2F). While northwesterly shamal winds have weakened over the AG during both winter and summer, surface winds over the SOO have weakened during winter and increased during summer, contributing to the differential warming in the region in recent decades (Fig 2 and Fig S13, SI).

4 Discussion

4.1 Comparison with previous works

Our study reveals significant variability in the exchange flow between the AG and the SOO, primarily driven by fluctuations in atmospheric forcing over the AG. This finding aligns with the research conducted by Lorenz et al. (2020) and Pous et al. (2015), who concluded that interannual variability in Gulf outflow is primarily influenced by surface fluxes.

We found the warming rate of the Gulf to be on average around 0.26°C per decade but with a strong spatiotemporal variability with local warming rates ranging from less than 0.2°C per decade in winter to above 0.5°C per decade during summer in much of the western Gulf. Other studies also reported important warming in the Gulf with rates varying between 0.2°C and 0.7°C depending on the region and period considered (Al-Rashidi et al., 2009; Hereher, 2020; Al Senafi, 2022). Bordbar et al. (2024) analyzed the variability in surface temperature and chlorophyll-a using MODIS-Aqua satellite data between 2003 and 2021 for the AG and the SOO region. Overall, they found no significant trend in the time series of chlorophyll in the Gulf over the study period. Interestingly, they found no major difference in the summer warming rates in the AG and the

SOO and only a slightly faster warming in the AG on an annual mean. When considering a similar period (2003-2018), we also found no significant trend in either chlorophyll-a levels, primary production or temperature gradient between the two seas. This suggests that the long-term trends reported in this study cannot be discerned from the shorter period covered by sea color satellite data.

Finally, in a recent modeling study, Vasou et al. (2024) studied the changes in the heat content of the AG over the period between 1993 and 2021. While they showed that the interannual variability in the heat content is dominated by the surface heat fluxes, they also suggested that the long-term warming of the basin is primarily driven by enhanced heat transport from the Arabian Sea because of a simulated increase in the annual mean volume of waters being exchanged at the Strait. Contrary to Vasou et al. (2024), our findings indicate that long-term warming trends in the AG are driven by changes in atmospheric heat fluxes, similar to seasonal and interannual variability. We did not observe an increase in the overturning circulation of the AG. Instead, we found a significant decrease in the volume of Gulf outflow in summer and only a slight increase in winter. This aligns with the warming-induced reduction in density contrasts between the two seas, the primary determinant of outflow strength according to theory (e.g., Bryden & Stommel, 1984; Pratt & Lundberg, 1991) and previous studies of the Gulf circulation (e.g., Swift & Bower, 2003; Kämpf & Sadrinasab, 2006; Pous et al., 2015; Lorenz et al., 2020; Paparella et al., 2022). The recent decrease in density gradient and exchange strength is further corroborated by evidence from ORAS5 reanalysis and multiple versions of the SODA reanalysis, all indicating a notable reduction in density contrast between the AG and the SOO, along with decreased Gulf outflow intensity in recent decades, particularly pronounced in summer (Fig S14, SI). It is important to mention that simulated surface temperature trends in Vasou et al. (2024) significantly underestimate observed trends in the AG and overestimate them in the SOO (refer to their Figure S1).

4.2 Caveats and limitations

While large-scale changes in atmospheric conditions in the Gulf region are relatively robust across multiple data-based products (Fig 2 and Fig S13, SI), they still harbor significant uncertainties, particularly at smaller, local scales. These uncertainties arise from the limited availability of direct observations and the relatively low spatial resolution of existing atmospheric forcing products. To enhance confidence in modeling the AG circulation and biogeochemical changes, it is important to employ better-resolved atmospheric forcing, validated via local in-situ observations, in future studies. Furthermore, the simulated alterations in Gulf outflow, productivity, and nutrient availability require confirmation through in-situ observations. Repeated measurements of critical physical parameters, such as the intensity of water exchange through the Strait, and vital biological parameters, such as chlorophyll and nutrient concentrations, are essential for documenting ongoing changes in this region, which is both under-sampled and under-studied.

4.3 Implications and recommendations

Our findings indicate that both the physical and biogeochemical properties of the Gulf exhibit significant variability across seasons and years. Consequently, measurements taken over short periods may not accurately capture the climatological conditions in the AG. This highlights the importance of employing high-resolution monitoring or continuous sampling methods, such as through the use of oceanographic moorings. Moreover, the monitoring of key variables, such as the strength of the Gulf outflow, is particularly crucial due to its critical role in the ecology and biogeochemistry of the Gulf, as evidenced in this study. The demonstrated strong relationship between Gulf outflow variability and density contrasts between the two seas underscores the potential for monitoring this gradient as a proxy to gain insights into exchange flux and its variability. The export and subsequent subduction of the Gulf waters in the northern Arabian Sea has been shown to deeply affect the intensity of the Arabian Sea oxygen minimum zone and hence the biogeochemistry of the northern Indian Ocean (Lachkar et al., 2019, 2021; Ditkovsky et al., 2023). Here, we show that a reduction of the Gulf outflow also deeply affects the biogeochemistry of the Gulf itself.

The findings of this study have important implications for biodiversity and socioeconomics in the Gulf. As a marginal marine system characterized by already extreme environmental conditions (Burt et al., 2020), further pressures such as those identified here have great potential to result in sudden, non-linear impacts on marine organisms and ecosystems (Bouwmeester et al., 2020). Marine organisms in the Gulf are considered to live very near to their thermal tolerance thresholds in summer, and we are already witnessing an increasing frequency and severity of coral bleaching and mass mortality events during summers when low wind conditions permit temperatures to rise by just 2°C above the normal summer maximum (Burt et al., 2019; Riegl et al., 2018). As ectothermic fauna whose metabolic oxygen demand is directly tied to temperature, fishes are likely to face considerable physiological strain from the need to consume more oxygen under extreme temperatures while simultaneously being challenged by the growing extent of hypoxia that has been identified in the Gulf (Vaughan et al., 2021; de Verneil et al., 2021; Lachkar et al., 2022). The physiological costs of accommodating the naturally extreme temperatures and salinity in the Gulf have previously been implicated in reducing the size and productivity of Gulf fish and therefore fisheries yields (Ben-Hasan et al., 2024); further environmental pressure may exacerbate these effects and have direct negative impacts on fisheries - a resource sector second only to oil in this region (Van Lavieren et al., 2011).

5 Summary and Conclusions

As a shallow, semi-enclosed marginal sea, the AG is notably sensitive to atmospheric forcing, leading to heightened seasonal and interannual variability compared to the SOO. Our analysis confirms that the AG has experienced rapid warming, exceeding that of the neighboring SOO. The primary driver of warming in both seas is enhanced downward radiation. However, weakening winds over the AG and strengthened southeasterly winds over the SOO contribute to accelerating warming in the former and dampening it in the latter. Consequently, this process increases the temperature gradient and reduces the density gradient between the two seas, thereby slowing down the water exchange between the Gulf and the Arabian Sea. This reduction in Gulf water outflow has led to an increased accumulation of nutrients and biomass in the Gulf over the recent decades, intensifying respiration and causing depletion of O_2 and an increase in water acidity, particularly pronounced in the deeper parts of the Gulf. Our findings underscore the importance of local changes in atmospheric conditions, particularly surface winds, in modulating global anthropogenic perturbations at regional scales, particularly for marginal and semi-enclosed seas.

6 Open Research

The ERA-Interim data used for forcing the model atmospheric boundary condition is available at: `https://rda.ucar.edu/datasets/ds627.2/dataaccess/`. The ORAS5 data used for forcing the lateral boundary condition is available at: `https://cds.climate.copernicus.eu/cdsapp#!/dataset/reanalysis-oras5?tab=overview`. The model code (croco v1.0) can be accessed online (`https://gitlab.inria.fr/croco-ocean/croco/-/releases`). The model outputs are available online at `https://zenodo.org/records/10987332`.

Acknowledgments

This research was supported by funding provided by Tamkeen through grants CG009 to the Mubadala ACCESS center and CG007 to the Water Research Center, as well as funding support from Mubadala Philanthropies under XR016; their support is greatly appreciated. Computations were performed at the High Performance Computing (HPC) cluster of NYUAD, Jubail. We extend thanks to the NYUAD HPC team for technical support.

References

Al-Ansari, E. M., Rowe, G., Abdel-Moati, M., Yigiterhan, O., Al-Maslamani, I., Al-Yafei, M., … Upstill-Goddard, R. (2015). Hypoxia in the central arabian gulf exclusive economic zone (eez) of qatar during summer season. *Estuarine, Coastal and Shelf Science*, *159*, 60–68.

Al-Rashidi, T. B., El-Gamily, H. I., Amos, C. L., & Rakha, K. A. (2009). Sea surface temperature trends in kuwait bay, arabian gulf. *Natural Hazards*, *50*(1), 73–82.

Al Senafi, F. (2022). Atmosphere-ocean coupled variability in the arabian/persian gulf. *Frontiers in Marine Science*, *9*, 809355.

Al-Yamani, F., & Naqvi, S. (2019). Chemical oceanography of the arabian gulf. *Deep Sea Research Part II: Topical Studies in Oceanography*, *161*, 72–80.

Ben-Hasan, A., Vahabnezhad, A., Burt, J. A., Alrushaid, T., & Walters, C. J. (2024). Fishery implications of smaller asymptotic body size: Insights from fish in an extreme environment. *Fisheries Research*, *271*, 106918.

Bordbar, M. H., Nasrolahi, A., Lorenz, M., Moghaddam, S., & Burchard, H. (2024). The persian gulf and oman sea: Climate variability and trends inferred from satellite observations. *Estuarine, Coastal and Shelf Science*, *296*, 108588.

Bouwmeester, J., Riera, R., Range, P., Ben-Hamadou, R., Samimi-Namin, K., & Burt, J. (2020). Coral and reef fish communities in the thermally extreme persian/arabian gulf: insights into potential climate change effects. *Perspectives on the marine animal forests of the world*, 63–86.

Bryden, H., & Stommel, H. (1984). Limiting processes that determine basic features of the circulation in the mediterranean-sea. *Oceanologica acta*, *7*(3), 289–296.

Burt, J. A., Camp, E., Enochs, I., Johansen, J., Morgan, K., Riegl, B., & Hoey, A. (2020). Insights from extreme coral reefs in a changing world. *Coral Reefs*, *39*, 495–507.

Burt, J. A., & Paparella, F. (2023). The marine environment of the emirates. In *A natural history of the emirates* (pp. 95–117). Springer.

Burt, J. A., Paparella, F., Al-Mansoori, N., Al-Mansoori, A., & Al-Jailani, H. (2019). Causes and consequences of the 2017 coral bleaching event in the southern persian/arabian gulf. *Coral Reefs*, *38*(4), 567–589.

Chao, S.-Y., Kao, T. W., & Al-Hajri, K. R. (1992). A numerical investigation of circulation in the arabian gulf. *Journal of Geophysical Research: Oceans*, *97*(C7), 11219–11236.

de Verneil, A., Burt, J. A., Mitchell, M., & Paparella, F. (2021). Summer oxygen dynamics on a southern arabian gulf coral reef. *Frontiers in Marine Science*, 1676.

de Verneil, A., Lachkar, Z., Smith, S., & Lévy, M. (2022). Evaluating the arabian sea as a regional source of atmospheric co 2: seasonal variability and drivers. *Biogeosciences*, *19*(3), 907–929.

Ditkovsky, S., Resplandy, L., & Busecke, J. (2023). Unique ocean circulation pathways reshape the indian ocean oxygen minimum zone with warming. *Biogeosciences*, *20*(23), 4711–4736.

Garcia, H., Boyer, T., Baranova, O., Locarnini, R., Mishonov, A., Grodsky, A. e., ... others (2019). World ocean atlas 2018: Product documentation. *A. Mishonov, Technical Editor*.

Gruber, N., Frenzel, H., Doney, S. C., Marchesiello, P., McWilliams, J. C., Moisan,

J. R., . . . Stolzenbach, K. D. (2006). Eddy-resolving simulation of plankton ecosystem dynamics in the california current system. *Deep Sea Research Part I: Oceanographic Research Papers*, *53*(9), 1483–1516.

Hereher, M. E. (2020). Assessment of climate change impacts on sea surface temperatures and sea level rise—the arabian gulf. *Climate*, *8*(4), 50.

Izumi, C., Al-Thani, J. A., Yigiterhan, O., Al-Ansari, E. M. A., Vethamony, P., Sorino, C. F., . . . Murray, J. W. (2022). Excess pco2 and carbonate system geochemistry in surface seawater of the exclusive economic zone of qatar (arabian gulf). *Marine Chemistry*, *247*, 104185.

Johns, W., Yao, F., Olson, D., Josey, S., Grist, J., & Smeed, D. (2003). Observations of seasonal exchange through the straits of hormuz and the inferred heat and freshwater budgets of the persian gulf. *Journal of Geophysical Research: Oceans*, *108*(C12).

Joos, F., & Spahni, R. (2008). Rates of change in natural and anthropogenic radiative forcing over the past 20,000 years. *Proceedings of the National Academy of Sciences*, *105*(5), 1425–1430.

Kämpf, J., & Sadrinasab, M. (2006). The circulation of the persian gulf: a numerical study. *Ocean Science*, *2*(1), 27–41.

Keeling, C. D., Piper, S. C., Bacastow, R. B., Wahlen, M., Whorf, T. P., Heimann, M., & Meijer, H. A. (2005). Atmospheric co2 and 13co2 exchange with the terrestrial biosphere and oceans from 1978 to 2000: observations and carbon cycle implications. In *A history of atmospheric co2 and its effects on plants, animals, and ecosystems* (pp. 83–113). Springer.

Lachkar, Z., Lévy, M., & Smith, K. (2019). Strong intensification of the arabian sea oxygen minimum zone in response to arabian gulf warming. *Geophysical Research Letters*, *46*(10), 5420–5429.

Lachkar, Z., Mehari, M., Al Azhar, M., Lévy, M., & Smith, S. (2021). Fast local warming is the main driver of recent deoxygenation in the northern arabian sea. *Biogeosciences*, *18*(20), 5831–5849.

Lachkar, Z., Mehari, M., Levy, M., Paparella, F., & Burt, J. A. (2022). Recent expansion and intensification of hypoxia in the arabian gulf and its drivers. *Frontiers in Marine Science*, *9*, 891378.

Large, W. G., McWilliams, J. C., & Doney, S. C. (1994). Oceanic vertical mixing: A review and a model with a nonlocal boundary layer parameterization. *Reviews of Geophysics*, *32*(4), 363–403.

Lauvset, S. K., Key, R. M., Olsen, A., Van Heuven, S., Velo, A., Lin, X., ... others (2016). A new global interior ocean mapped climatology: The 1× 1 glodap version 2. *Earth System Science Data*, *8*(2), 325–340.

Lorenz, M., Klingbeil, K., & Burchard, H. (2020). Numerical study of the exchange flow of the persian gulf using an extended total exchange flow analysis framework. *Journal of Geophysical Research: Oceans*, *125*(2), e2019JC015527.

Naqvi, S., Sarma, V., & Jayakumar, D. (2002). Carbon cycling in the northern arabian sea during the northeast monsoon: Significance of salps. *Marine Ecology Progress Series*, *226*, 35–44.

Paparella, F., D'Agostino, D., & A. Burt, J. (2022). Long-term, basin-scale salinity impacts from desalination in the arabian/persian gulf. *Scientific reports*, *12*(1), 20549.

Paparella, F., Xu, C., Vaughan, G. O., & Burt, J. A. (2019). Coral bleaching in the persian/arabian gulf is modulated by summer winds. *Frontiers in Marine Science*, *6*, 205.

Pous, S., Lazure, P., & Carton, X. (2015). A model of the general circulation in the persian gulf and in the strait of hormuz: Intraseasonal to interannual variability. *Continental Shelf Research*, *94*, 55–70.

Pratt, L., & Lundberg, P. (1991). Hydraulics of rotating strait and sill flow. *Annual Review of Fluid Mechanics*, *23*(1), 81–106.

Purkis, S. J., Renegar, D., & Riegl, B. (2011). The most temperature-adapted corals have an achilles' heel. *Marine pollution bulletin*, *62*(2), 246–250.

Reynolds, R. M. (1993). Physical oceanography of the gulf, strait of hormuz, and the gulf of oman—results from the mt mitchell expedition. *Marine Pollution Bulletin*, *27*, 35–59.

Riegl, B., Johnston, M., Purkis, S., Howells, E., Burt, J., Steiner, S. C., ... Bauman, A. (2018). Population collapse dynamics in acropora downingi, an arabian/persian gulf ecosystem-engineering coral, linked to rising temperature. *Global change biology*, *24*(6), 2447–2462.

Saleh, A., Abtahi, B., Mirzaei, N., Chen, C.-T. A., Ershadifar, H., Ghaemi, M., ... Abedi, E. (2021). Hypoxia in the persian gulf and the strait of hormuz.

Marine Pollution Bulletin, *167*, 112354.

Shchepetkin, A. F., & McWilliams, J. C. (2005). The regional oceanic modeling system (roms): a split-explicit, free-surface, topography-following-coordinate oceanic model. *Ocean modelling*, *9*(4), 347–404.

Strong, A. E., Liu, G., Skirving, W., & Eakin, C. M. (2011). Noaa's coral reef watch program from satellite observations. *Annals of GIS*, *17*(2), 83–92.

Swift, S. A., & Bower, A. S. (2003). Formation and circulation of dense water in the persian/arabian gulf. *Journal of Geophysical Research: Oceans*, *108*(C1), 4–1.

Thoppil, P. G., & Hogan, P. J. (2009). On the mechanisms of episodic salinity outflow events in the strait of hormuz. *Journal of Physical Oceanography*, *39*(6), 1340–1360.

Uddin, S., Gevao, B., Al-Ghadban, A., Nithyanandan, M., & Al-Shamroukh, D. (2012). Acidification in arabian gulf–insights from ph and temperature measurements. *Journal of Environmental Monitoring*, *14*(5), 1479–1482.

Van Lavieren, H., Burt, J., Feary, D., Cavalcante, G., Marquis, E., Benedetti, L., … Sale, P. (2011). Managing the growing impacts of development on fragile coastal and marine ecosystems: Lessons from the gulf.

Vasou, P., Krokos, G., Langodan, S., Sofianos, S., & Hoteit, I. (2024). Contribution of surface and lateral forcing to the arabian gulf warming trend.

Vaughan, G. O., Al-Mansoori, N., & Burt, J. A. (2019). The arabian gulf. In *World seas: An environmental evaluation* (pp. 1–23). Elsevier.

Vaughan, G. O., Shiels, H. A., & Burt, J. A. (2021). Seasonal variation in reef fish assemblages in the environmentally extreme southern persian/arabian gulf. *Coral Reefs*, *40*(2), 405–416.

Yao, F., & Johns, W. E. (2010). A hycom modeling study of the persian gulf: 2. formation and export of persian gulf water. *Journal of Geophysical Research: Oceans*, *115*(C11).

Zuo, H., Balmaseda, M. A., Tietsche, S., Mogensen, K., & Mayer, M. (2019). The ecmwf operational ensemble reanalysis–analysis system for ocean and sea ice: a description of the system and assessment. *Ocean science*, *15*(3), 779–808.

Figure 2. Warming and surface wind changes in the AG and SOO. (A) Average summer (JJA) sea surface temperature (SST; in °C) in the northern Arabian Sea as simulated in the model over the study period (1980-2018). (B) Linear trends in summer (JJA) SST (in °C per decade) in the AG and northern Arabian Sea. (C-D) Trends in AG-averaged SST (C) and SST gradient between the AG and the SOO (D) during winter (blue), summer (red) and anual-mean (purple) based on the ROMS simulation and from different data products. (E-F) Trends in AG-averaged surface wind speed (E) and the difference in surface wind speed trends between the AG and the SOO (F) during winter (blue), summer (red) and for the month of August (pink) based on different atmospheric reanalyses products. White stars and triangles indicate statistically significant trends at 95% and 90% confidence levels, respectively.

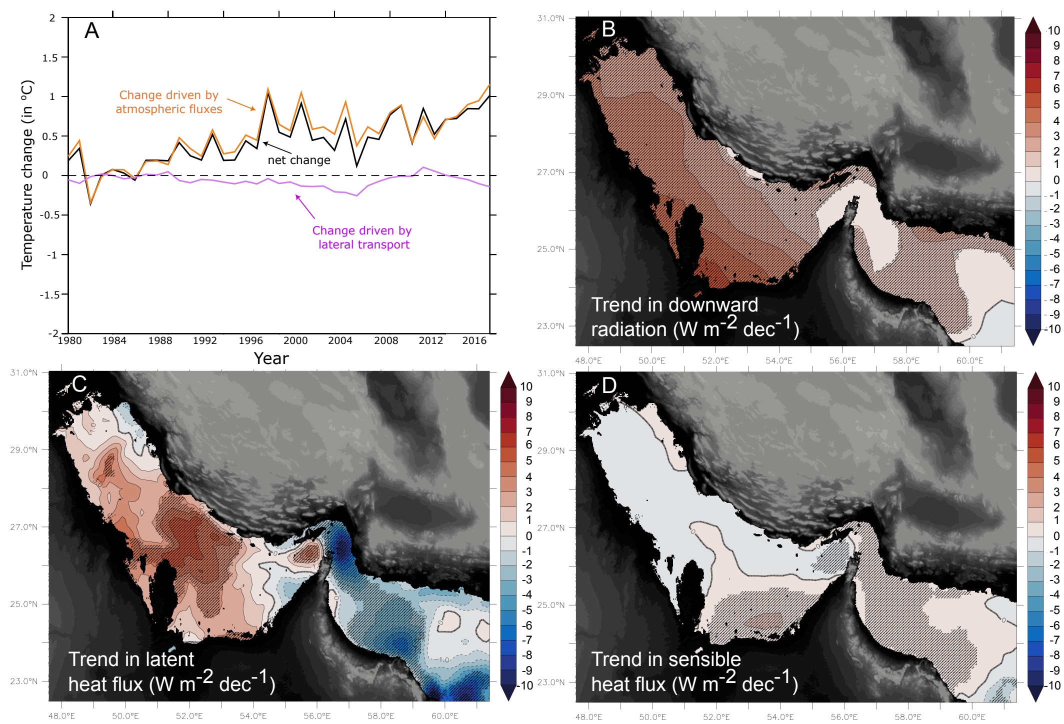

Figure 4. Drivers of AG warming. (A) Heat budget in the AG showing the contribution of atmospheric fluxes (orange) and lateral fluxes (magenta) to the net temperature change (black) over the study period. (B-D) Trends in downward radiation (B), latent (C) and sensible (D) heat fluxes over the study period (in W m^{-2} per decade; positive fluxes indicate ocean heat gain). Hatching indicates areas where trends are statistically significant at 95% confidence level.

Supporting Information for "Acceleration of warming, deoxygenation and acidification in the Arabian Gulf driven by weakening of summer winds"

Z. Lachkar[1], M. Mehari[1,*], F. Paparella[1], J. A. Burt[1,2]

[1]Mubadala Arabian Center for Climate and Environmental Sciences, New York University Abu Dhabi, Abu Dhabi, United Arab Emirates

[2]Water Research Center, New York University Abu Dhabi, Abu Dhabi, United Arab Emirates

[*]Now at: Global Modeling and Assimilation Office, Science Applications International Corporation, National Aeronautics and Space Administration Goddard Space Flight Center, Greenbelt, MD, USA

Contents of this file

1. Text S1: description of the model setup

The circulation model is based on the Regional Ocean Modeling System (ROMS) (Shchepetkin & McWilliams, 2005). Advection is formulated using a rotated-split thirdorder upstream biased operator as described by Marchesiello, Debreu, and Couvelard (2009), while vertical mixing is represented using the non-local K-profile parameterization (KPP) scheme proposed by Large, McWilliams, and Doney (1994). The model's domain spans the Indian Ocean from 31.5°S to 31°N and 30°E to 120°E, with a horizontal resolution of 1/10° and 32 sigma-coordinate vertical layers, featuring enhanced resolution near the surface. Biogeochemical processes are simulated using a nitrogen-based nutrient, phytoplankton, zooplankton, detritus (NPZD) model, comprising two nutrient components (nitrate and ammonium), one phytoplankton, one zooplankton, and two detrital classes (Gruber et al., 2006). Previous observations highlight nitrogen as the primary limiting nutrient in the Gulf, justifying the adoption of a nitrogen-based NPZD model to explore Gulf biogeochemistry dynamics (Quigg et al., 2013; Al-Said et al., 2018; Al-Yamani & Naqvi, 2019). Furthermore, the model incorporates a module describing the oxygen cycle (Lachkar et al., 2021). At suboxic oxygen concentrations ($O_2 < 4$ mmol m^{-3}) nitrification halts, and the remineralization rate is reduced by half. Additionally, aerobic remineralization of detritus is replaced by water column denitrification, where nitrate substitutes oxygen as the electron acceptor. Benthic denitrification is also accounted for in the model, following the parameterization by (Middelburg et al., 1996). Additional details regarding the implementation of denitrification in the model are provided in Lachkar, Smith, Lévy, and Pauluis (2016). The model incorporates a carbon module comprising three state variables: dissolved inorganic carbon (DIC), total alkalinity (TA), and calcium carbonate (Lachkar & Gruber, 2013; Lachkar, 2014; de Verneil et al., 2022). Organic carbon is linked to organic nitrogen through the Redfield ratio of 106:16. Surface fluxes of

DIC and TA, propelled by variations in sea surface salinity, are included as virtual fluxes that scale proportionally with the sea surface salinity forcing. Carbonate chemistry is computed using routines from the Ocean Carbon-Cycle Model Intercomparison Project (OCMIP) (Orr et al., 2005). The formulation of air-sea gas transfer adopts a quadratic wind speed dependence as delineated by Wanninkhof (1992). Comprehensive details of the biogeochemical model are provided in Lachkar et al. (2021); de Verneil et al. (2022).

The hindcast simulation is forced by ECMWF ERA-Interim 6-hourly heat fluxes, air temperature, pressure, humidity, precipitation, and winds spanning the period from January 1980 to December 2018. Initial and lateral boundary conditions for temperature, salinity, currents, and sea surface height are derived from the ECMWF Ocean Reanalysis System 5 (ORAS5; Zuo et al., 2019). Nitrate and oxygen initial and lateral boundary conditions are based on World Ocean Atlas 2018 (Garcia et al., 2019). Initial and lateral boundary conditions for DIC and TA are obtained from GLODAP version 2 (Lauvset et al., 2016). Atmospheric pCO_2 is prescribed using monthly data from Mauna Loa (Keeling et al., 2005), while atmospheric CO_2 data preceding 1958 is extracted from Joos and Spahni (2008). Riverine inputs include nutrients (Krishna et al., 2016; Ramesh et al., 1995) but exclude carbon or alkalinity. To accommodate the accumulation of anthropogenic carbon at the open lateral boundaries during the simulation period, decadally-varying DIC is utilized, derived from available estimates of anthropogenic CO_2 (Key et al., 2004; Gruber et al., 2019; Olsen et al., 2019) regressed against atmospheric CO_2 concentrations. Initial and boundary conditions for DIC and TA are processed in accordance with de Verneil et al. (2022) to incorporate a seasonal cycle in the upper ocean.

The model is first spun up for an initial 30 years with a repeated normal year (neutral with respect to major climate variability modes; 1984) forcing for heat, freshwater and momentum fluxes but with increasing atmospheric CO_2 concentrations and DIC at the atmospheric and lateral boundaries (to represent the increasing carbon levels in the atmosphere and the ocean between 1950 and 1979) and is then run for a complete 39-year (1980-2018) forcing cycle where both atmospheric physical fluxes as well as carbon vary annually following observations (i.e., the total duration of the spin-up phase is 69 years). Following the spin-up phase, the model undergoes an additional forcing cycle, constituting the hindcast run (HR) used for analysis. This is similar to the forcing protocol used in the the CORE-II simulations and the Ocean Model Intercomparison Project (Griffies et al., 2016). Adhering to the recommendations of the RECCAP2 protocol, the spin-up run (characterized by climatological forcing and increasing CO_2) is extended to cover the same period (1980-2018) as the HR. This simulation, termed Constant Climate (CC hereafter), serves to quantify any artificial trends in circulation and biogeochemistry solely induced by model drift and contrasts them with trends estimated in the HR. Furthermore, this simulation is employed to disentangle ocean acidification driven by rising anthropogenic CO_2 in the atmosphere from changes induced by alterations in climate, ocean circulation, and biology.

2. Text S2: evaluation of model drift

To assess the potential impact of model drift on our findings, we examined the trends in several key variables within the CC simulation and compared them with those in the HR simulation. Given that all forcing, except CO_2, is climatological in CC, any long-term changes in variables other than CO_2 and associated variables (e.g., pH) within CC can be attributed to artificial trends stemming from model drift. Conversely, trends in CO_2 (and associated variables such as pH) in CC primarily result from the increasing anthropogenic CO_2 levels in the atmosphere. Contrasting these trends with those in HR enables us to gauge the influence of climate change and variability on carbon dynamics in the region. Table S1 presents the trends (1980-2018) in averaged physical (e.g., temperature, salinity, density, Gulf outflow) and biogeochemical (e.g., nitrogen transport through the Strait, net primary productivity, oxygen, and pH) properties in the AG from both simulations. This comparison highlights that the trends observed in CC are typically 1 to 3 orders of magnitude smaller than those in the HR simulation for all variables except pH. This suggests that model drift is negligible in the focus area and that the identified trends in the HR runs are primarily driven by changes in regional climatic conditions.

3. Text S3: evaluation of the model

The model effectively replicates the observed distributions of sea surface temperature (SST) obtained from NOAA Optimum Interpolation Sea Surface temperature (OISST) data, which combines satellite and in-situ (ships and buoys) measurements, during both winter and summer seasons (see Fig S1). Notably, the model accurately captures the pronounced temperature gradients present across the AG between its northwestern and southeastern regions as well as the temperature progression from winter to summer in the SOO. This favorable agreement for SST is somewhat anticipated, given that the model's simulated surface temperature is constrained by AVHRR satellite observations though restoring of surface temperature. To assess the model's performance in reproducing the three-dimensional structure of temperature and salinity within the region, we contrast our simulation with the limited historical observations available in the World Ocean Database (WOD) 2018 to bolster confidence in the simulated hydrography of the AG and the SOO.

For this purpose, we binned WOD observations monthly and on a 0.5x0.5 regular grid and regridded the model onto the same common grid. This comparison reveals that the model exhibits a similar range of variation in both temperature and salinity as depicted in the observations (see Fig S2 and Fig S3). Additionally, in both the AG and the SOO, modeled temperatures exhibit high correlations with WOD observations (R2 ranging between 0.84 in the SOO and 0.88 in the AG) and demonstrate limited systematic biases. Furthermore, the model accurately captures the seasonal temperature progression observed in WOD data for both surface and subsurface layers (Fig S2 and Fig S3). However, the model also exhibits some discrepancies compared to WOD observations, such as an overestimation of temperature by 1°C to 2°C at depth in the AG during summer and in the 100-200m layer in all seasons in the SOO. This disparity may partially stem from the fact that the model and observations cover slightly different time periods, with most WOD observations in the region collected in the period 1960-1995. While the variability range in both WOD and the model is similar in both seas, model tends to underestimate salinity in high-salinity (>39 psu) waters in the AG by up to 1 psu (see Fig S2). Similarly, the model underestimates WOD salinity in the SOO at depth (200-300m) by approximately 0.5 psu (Fig S3). However, the sparse observational coverage of WOD in the region, particularly for salinity where most available observations are extracted from a few individual years, implies that the WOD observations may not necessarily be representative of the long-term climatological conditions in the region (Fig S4). This is particularly pertinent given the strong seasonal and interannual variability characterizing temperature and salinity in the region, as demonstrated by the model simulations (see Fig 1).

The volume and seasonality of the Gulf's outflow via the Strait of Hormuz constitute an important parameter in our study. Johns et al. (2003) deployed acoustic Doppler current profiler (ADCP) moorings to measure the outflow's intensity and seasonal variations across the Strait of Hormuz between December 1996 to March 1998. The study identified a consistent and robust deep outflow below 45 meters, averaging 0.15 ± 0.03 Sv (where 1 Sv = 1 million cubic meters per second), fluctuating from 0.08 Sv in December to 0.18 Sv in March. Additionally, a more variable and weaker surface outflow of 0.06 ± 0.02 Sv was recorded above 45 meters. Our model simulates an annual deep outflow of 0.11 ± 0.06 Sv, ranging from 0.04 Sv in October to 0.15 Sv in March, and a surface outflow of 0.03 ± 0.02 Sv. The modeled annual outflow of 0.14 ± 0.07 Sv remains in agreement with Johns et al. (2003) estimate of 0.21 ± 0.05 Sv. Our model's results also align with prior estimates from indirect measurements and other model simulations (Table S2). In summary, despite some discrepancies, our model successfully captures the essential hydrographic features of the Arabian Gulf and Strait of Hormuz based on available data.

The evaluation of the model's ability to represent biological productivity is hindered by the lack of in-situ measurements of primary production and Chl-a pigment in the Gulf region. To address this, we compare our model's simulated chlorophyll-a levels to in-situ observations collected in the Qatar exclusive economic zone during six research cruises conducted between April 2015 and September 2016 (Al-Naimi et al., 2017). Our comparison shows a good agreement in surface chlorophyll concentration throughout the year, both in terms of annual average and seasonality (Fig S5). The model also accurately reproduces the depth and magnitude of the deep chlorophyll maximum (DCM) in spring and summer but underestimates it in winter and overestimates it in autumn (Fig S5). Additionally, satellite chlorophyll data from the Ocean Color Climate Change Initiative (OC-CCI) exhibit a significant correlation with in-situ observations in the region, despite a systematic overestimation of the latter (Figure 1, Al-Naimi et al., 2017). This overestimation is likely due to the high turbidity of Gulf waters and the presence of suspended sediments, which affect the reliability of satellite-derived chlorophyll estimates. Nevertheless, the strong correlation ($r = 0.795$, $p < 0.001$) between in-situ and satellite data suggests that remotely sensed chlorophyll observations can effectively characterize Gulf biological productivity seasonality (Al-Naimi et al., 2017). To further evaluate our model, we compare simulated net primary productivity (NPP) seasonal anomalies with data-based NPP estimates from the vertically generalized production model (VGPM) by Behrenfeld and Falkowski (1997) (Fig S6). This comparison demonstrates good agreement between the model and data-based NPP estimates across the Gulf, particularly in winter and summer seasons, highlighting the consistency of simulated NPP variability with satellite-based observations (Fig S6).

Observations of oxygen levels in the Gulf are scarce. In this study, we compare the model's simulated oxygen with data from an extensive survey conducted in the Iran exclusive economic zone (EEZ) from summer 2018 to autumn 2019 (Saleh et al., 2021). The comparison, illustrated in Figure S7, indicates that the model effectively captures the seasonal progression of low oxygen and bottom hypoxia, as indicated by the observations of Saleh et al. (2021). Specifically, oxygen levels were consistently lowest in late summer and early autumn (September) below 50 meters, while highest near the surface in May, both in the model and in the observations (Figure S7). Additionally, we compare key carbonate system parameters—DIC, TA, pCO_2, and pH—between the model and recent observations collected in December 2018 and May 2019 in the EEZ of Qatar by Izumi et al. (2022). With the exception of stations 1C and 2C, which are in close proximity to the coast and have shallow bathymetry not accurately represented in our model, DIC and TA exhibit good agreement with the collected data for both cruises (Fig S7). The model also shows good agreement with estimates of pCO_2 and pH for May 2019, but displays slightly larger discrepancies with respect to estimates from the December 2018 cruise. Nevertheless, the model reproduces the large-scale patterns of temporal and spatial variability observed in both variables. For instance, the higher pCO_2 levels observed in nearshore stations (1C, 2C, 3C) relative to those sampled farther offshore (4C, 5C, 6C, 6B) during May 2019, and the reverse pattern observed during December 2018, are both replicated in the model. Similarly, the lower pH recorded in nearshore stations compared to offshore stations in May 2019, and the opposite pattern observed in December 2018, are also reproduced in the model. In summary, our model's representation of biological production, oxygen levels, and the carbonate system aligns well with the available data, both in terms of the average range and the seasonal variability, as well as the large-scale spatial patterns.

Table S1. Trends under constant and varying climates. Trends (1980-2018) in AG-averaged sea surface temperature (in °C dec^{-1}), salinity (in psu dec^{-1}), density (in kg m^{-3} dec^{-1}), density gradient with the SOO (in kg m^{-3} dec^{-1}), Gulf outflow (in Sv dec^{-1}), transport of nitrogen through the Strait (in Gmol dec^{-1}), NPP (in g C m^{-2} yr^{-1} dec^{-1}), oxygen (in mmol m^{-3} dec^{-1}) and pH (in pH unit dec^{-1}) as simulated in the control HR and the constant climate (CC) simulations.

Simulation	Month	Temperature	Salinity	Density	Density gradient	Outflow	Transport of nitrogen	NPP	Oxygen (bottom)	$pH^{\perp}$ (bottom)
Control	Jan	0.108	0.014	-0.02	0.042	0.004	0.758	3.244	-0.41	-0.014
	Feb	0.17	0.006	-0.041	0.032	0.003	0.324	3.366	-0.912	-0.015
	Mar	0.352	-0.007	-0.102	-0.01	0.003	-1.108	2.406	-3.136	-0.019
	Apr	0.347	-0.003	-0.104	-0.008	0.002	-0.89	1.903	-3.344	-0.019
	May	0.358	0.002	-0.113	-0.035	-0.001	-0.855	2.207	-3.672	-0.02
	Jun	0.321	0.035	-0.082	-0.075	0	-0.158	3.129	-3.61	-0.02
	Jul	0.278	0.055	-0.057	-0.078	-0.002	0.821	3.239	-4.095	-0.021
	Aug	0.338	0.048	-0.086	-0.092	-0.004	0.418	2.824	-5.144	-0.022
	Sep	0.298	0.058	-0.063	-0.056	-0.007	1.583	3.859	-5.824	-0.023
	Oct	0.24	0.05	-0.046	-0.015	-0.003	0.746	5.754	-2.333	-0.018
	Nov	0.19	0.04	-0.032	0.02	-0.001	0.723	1.255	-0.119	-0.014
	Dec	0.105	0.025	-0.012	0.034	0.006	0.696	6.763	0.031	-0.013
Constant Climate	Jan	< 5e-4	< 5e-4	< 5e-4	0.001	< 5e-4	-0.139	0.397	0.006	-0.015
	Feb	-0.002	0.001	0.001	0.005	< 5e-4	-0.404	0.271	0.002	-0.015
	Mar	< 5e-4	0.001	< 5e-4	0.003	< 5e-4	0.087	0.245	0.006	-0.016
	Apr	< 5e-4	< 5e-4	< 5e-4	0.001	< 5e-4	0.145	0.409	0.024	-0.016
	May	< 5e-4	< 5e-4	< 5e-4	0.002	-0.001	0.147	0.453	-0.032	-0.016
	Jun	< 5e-4	< 5e-4	< 5e-4	0.004	< 5e-4	-0.028	0.424	-0.075	-0.016
	Jul	< 5e-4	< 5e-4	< 5e-4	0.002	0.001	-0.371	0.399	0.001	-0.017
	Aug	< 5e-4	< 5e-4	< 5e-4	0.003	< 5e-4	0.116	0.406	0.04	-0.017
	Sep	< 5e-4	< 5e-4	< 5e-4	< 5e-4	< 5e-4	0.068	0.398	0.036	-0.016
	Oct	< 5e-4	< 5e-4	< 5e-4	0.001	< 5e-4	0.065	0.479	0.02	-0.016
	Nov	< 5e-4	< 5e-4	< 5e-4	0.003	< 5e-4	0.016	0.399	0.073	-0.015
	Dec	< 5e-4	< 5e-4	< 5e-4	-0.001	< 5e-4	0.073	0.359	0.014	-0.015

Table S2. Gulf outflow estimates. Gulf inflow and outflow through the Strait of Hormuz (in Sv) as simulated in this study and from previous observation- and model-based estimates. The outflow is also separately estimated for shallow (depth above 45 m) and a deeper (depth below 45 m) layers following the description given by (Johns et al., 2003).

Study	Inflow	Outflow (total)	Outflow (deep)	Outflow (shallow)	Seasonality (Peak time/Minimum t
This study	0.15 ± 0.07	0.14 ± 0.07 [0.03-0.27]	0.11 ± 0.06	0.03 ± 0.02	May/October
(Johns et al., 2003)[†]	0.23 ± 0.04	0.21 ± 0.05	0.15 ± 0.03 [0.08-0.18]	0.06 ± 0.02	March/Decembe
(Pous et al., 2004)[‡]		0.21 [0.18-0.24]	0.16 [0.12-0.16]	0.01 [0-0.01]	NA[⋆]
(Ahmad & Sultan, 1991)[⊤]	0.19	0.17			NA[⋆]
(Chao et al., 1992)[⊥]		[0.03-0.17]			March/August
(Kämpf & Sadrinasab, 2006)[⊥]		[0.11-0.17]			spring/autumn
(Yao & Johns, 2010)[⊥]		[0.06-0.18]	[0.07-0.15]		July/January

† based on ADCP mooring

‡ based on geostrophic velocity estimates

⊤ based on a freshwater volume budget

⊥ based on numerical simulations

+ weak seasonality in deep outflow

⋆ NA = not available

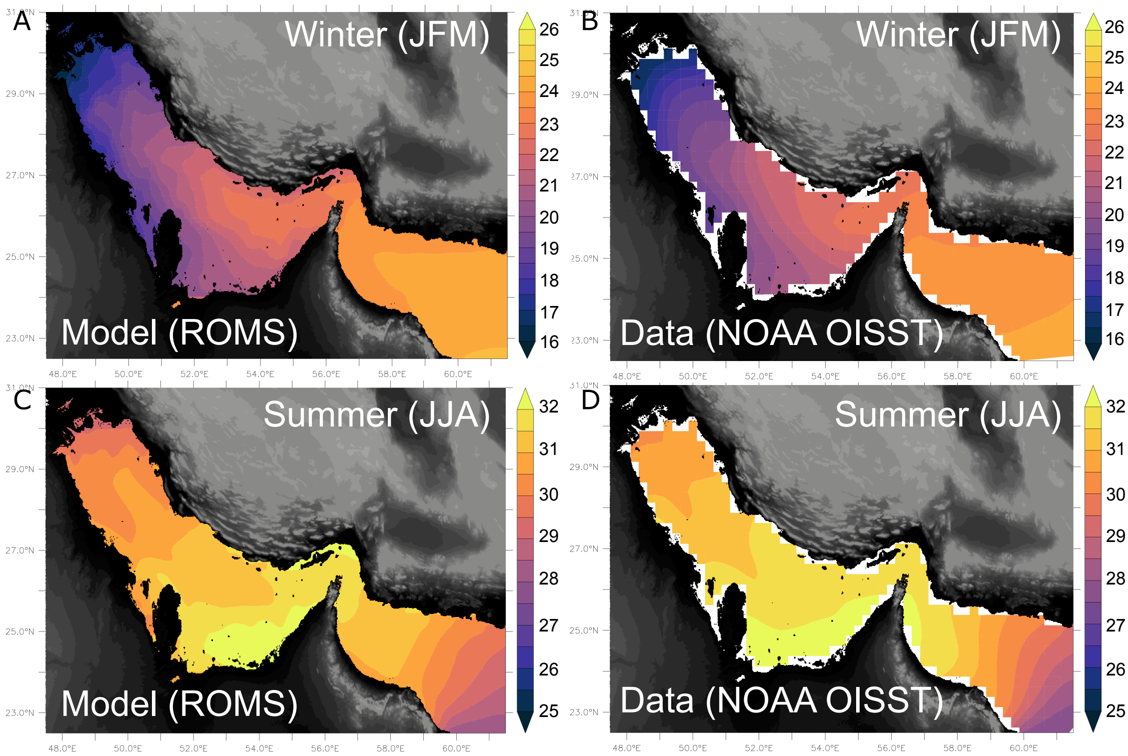

Figure S1. Evaluation of modeled sea surface temperature. Sea surface temperature as simulated (right) and from the NOAA Optimum Interpolation Sea Surface Temperature (OISST) data product (left) in winter (January-March, top panel) and summer (June-August, bottom panel).

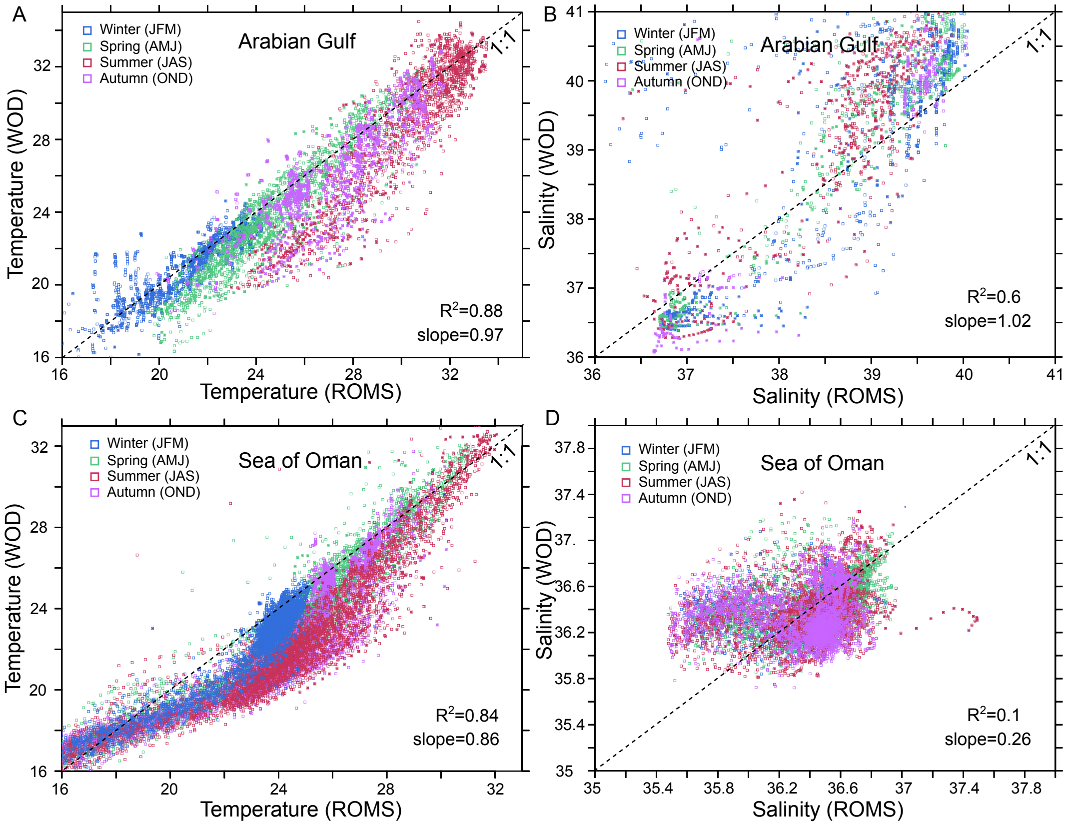

Figure S2. Comparison with WOD data for different seasons. Comparison between WOD observations and ROMS for temperature (left) and salinity (right) in the AG (top) and SOO (bottom) for different seasons.

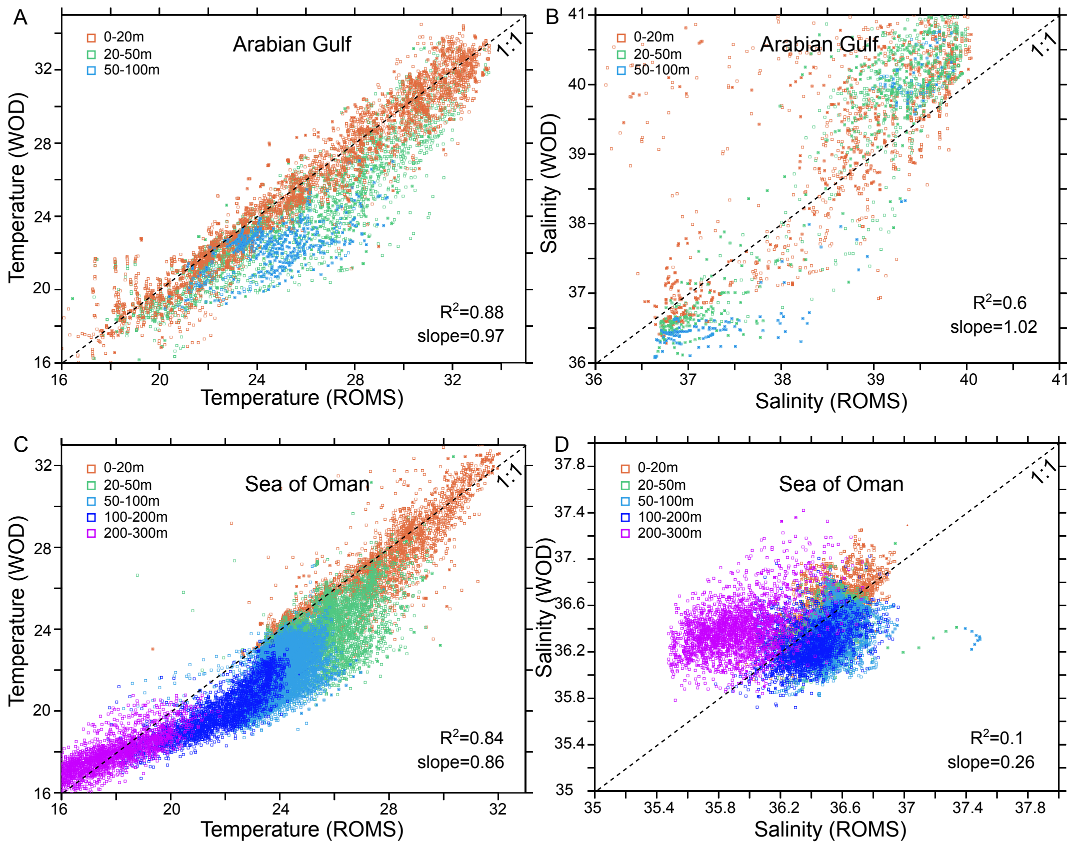

Figure S3. Comparison with WOD data for different vertical layers. Comparison between WOD observations and ROMS for temperature (left) and salinity (right) in the AG (top) and SOO (bottom) for different vertical layers.

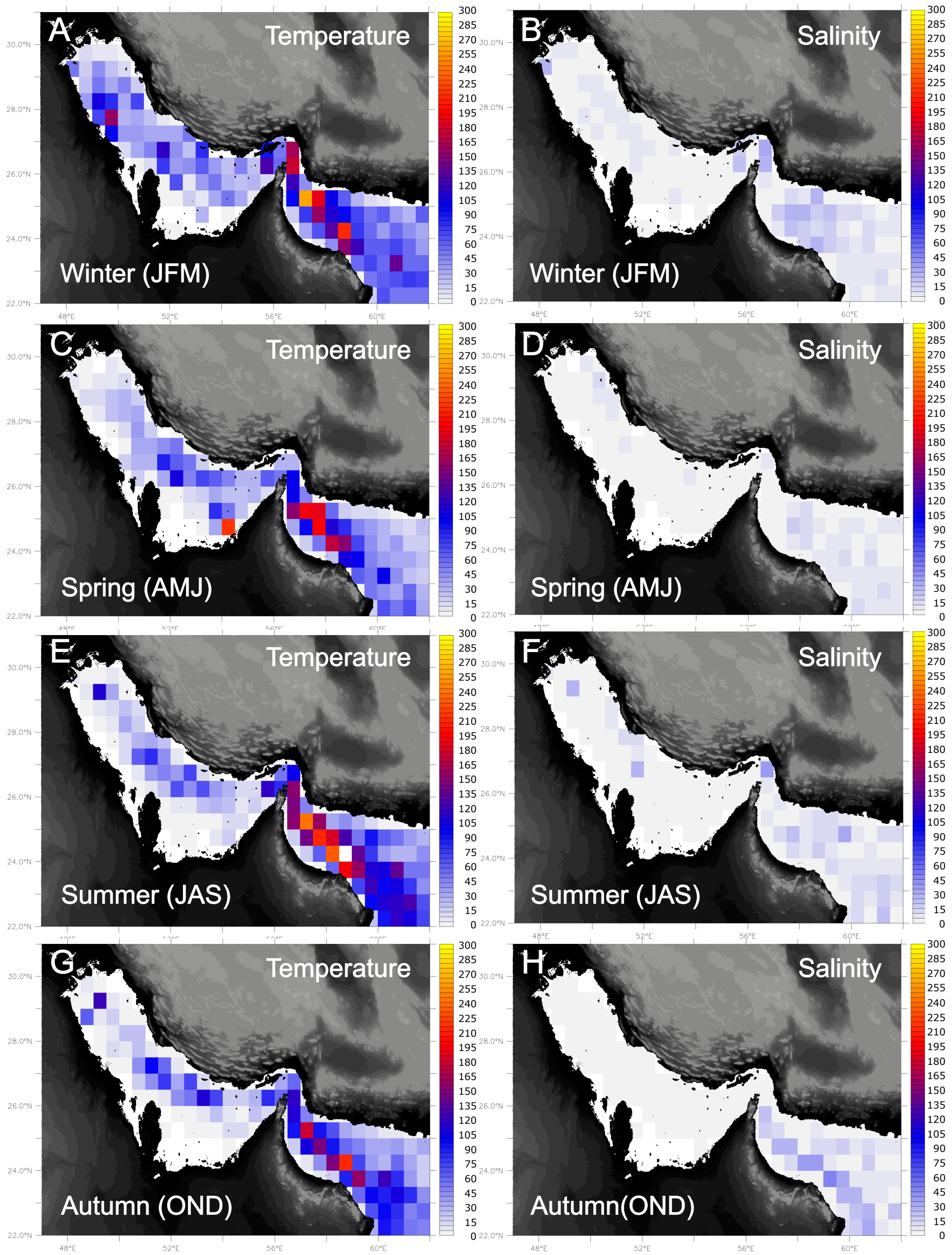

Figure S4. Number of observations. Number of available observed profiles in the World Ocean Database (2018) across the seasons in temperature (left) and salinity (right). Observations were binned on a monthly basis on a 0.5° x 0.5° regular grid. Model outputs were regridded on the same grid and sampled on observation grid points.

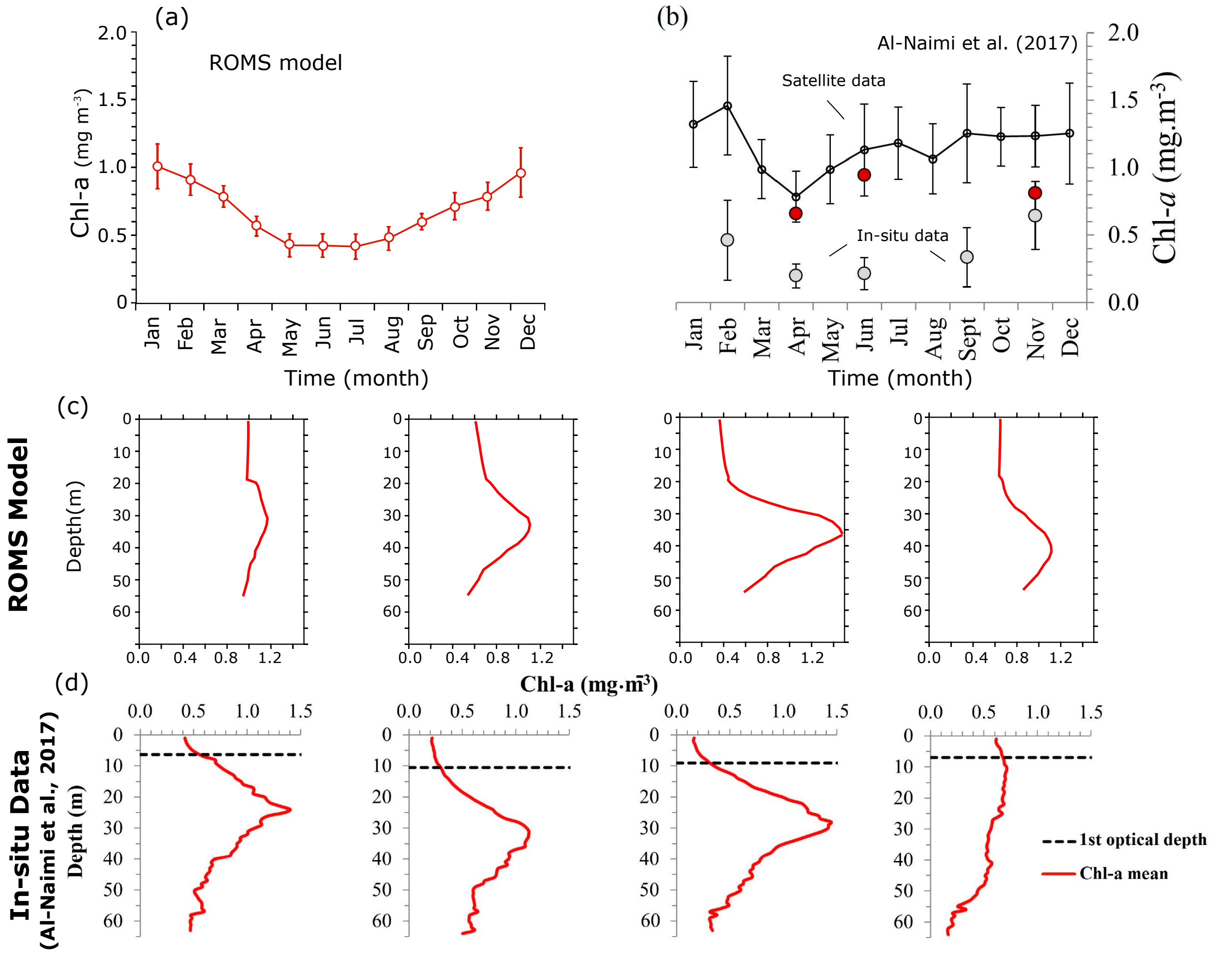

Figure S5. Evaluation of the model simulated chlorophyll-a concentrations. (a-b) Seasonal surface Chl-a concentrations (in mg m^{-3}) in the Qatar Exclusive Economic Zone (EEZ) (a) as simulated by ROMS and (b) from observations published by Al-Naimi et al. (2017). Gray circles show in-situ observations from six research cruises (2015-2016) while the black line indicates surface Chl-a based on the OC-CCI satellite monthly climatology (1997-2013). (c-d) Vertical profiles of Chl-a in the Qatar EEZ in winter (DJF), spring (MAM), summer (JJA) and autumn (SON) seasons as simulated by (c) ROMS and (d) from observations by Al-Naimi et al. (2017). Note that the seasonal in-situ chlorophyll profiles for winter, spring, summer and autumn are based on data collected in February 2016, April 2015/2016, June 2015, and September 2016/November 2015, respectively.

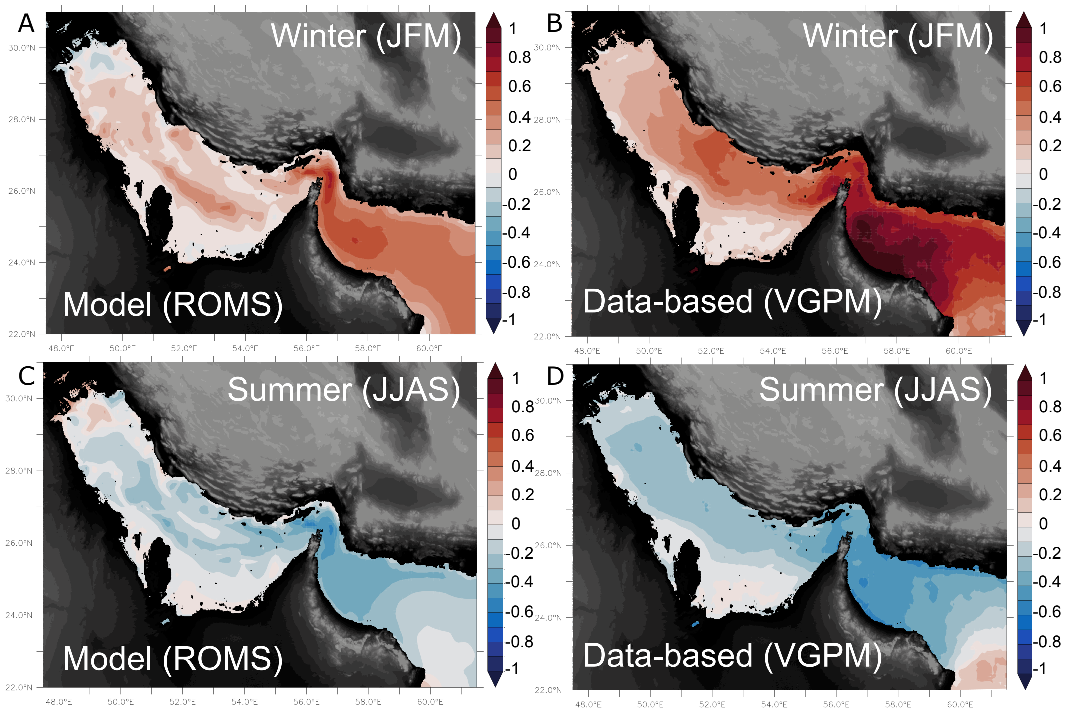

Figure S6. Evaluation of model simulated NPP seasonal variability. Seasonal anomalies in NPP (in g C m^{-2} yr^{-1}) in winter (top) and summer (bottom) as simulated by the model (left) and as estimated from satellite data based on the Vertically Generalized Production Model (VGPM) of Behrenfeld and Falkowski (1997) (right).

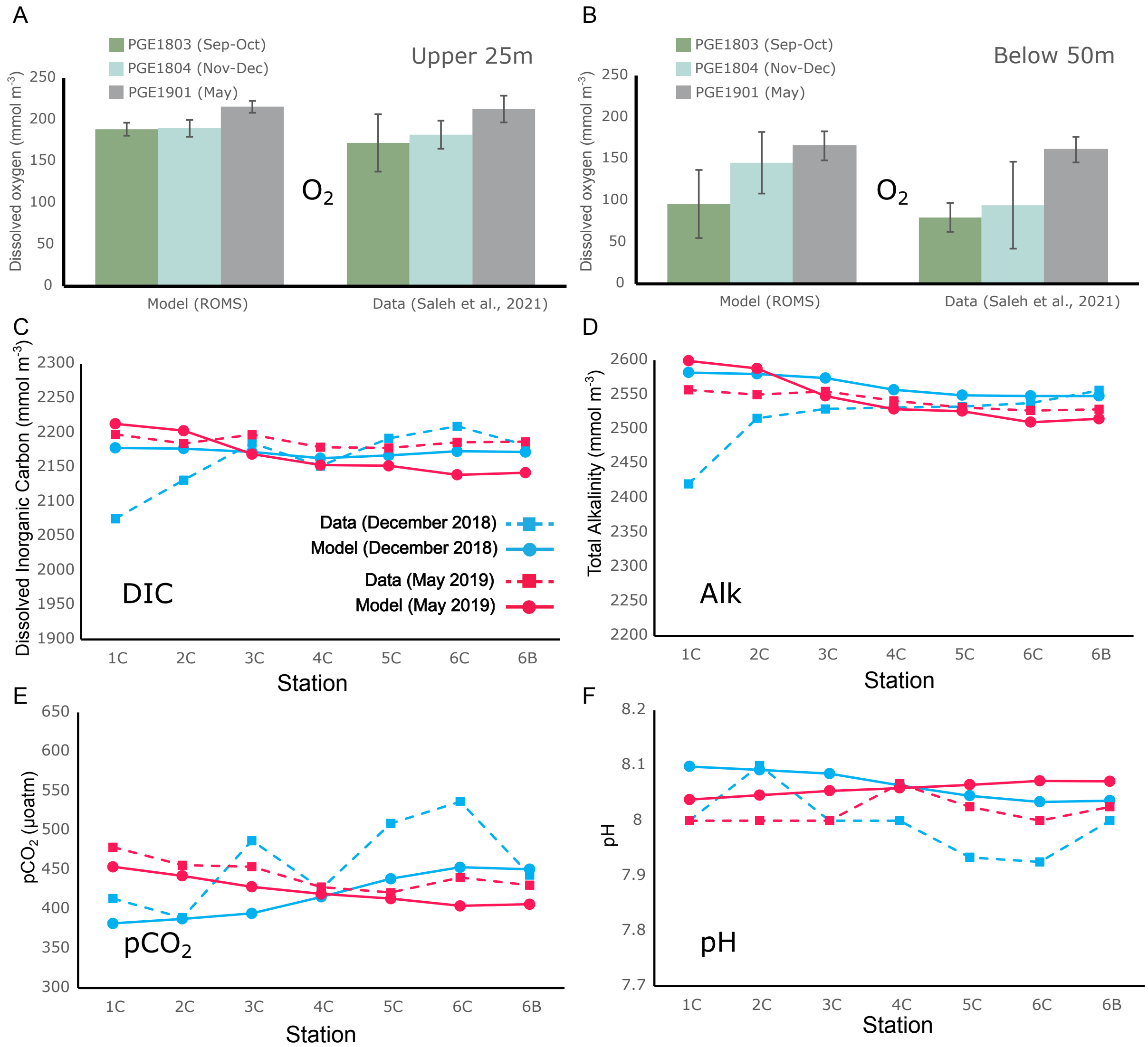

Figure S7. **Comparison of simulated O_2 and carbon to available observations** . (A-B) Comparison of the model simulated dissolved O_2 concentrations in the the AG (Iran EEZ) to observations collected during cruises PGE1803 (late summer), PGE1804 (late autumn), PGE1901, and PGE1902 (spring) in 2018 and 2019 by Saleh et al. (2021) in the upper 25m (A) and below 50m (B). Bar plots correspond to average concentrations for each cruise while error bars show standard deviations around the mean. (C-D) Comparison of the model simulated (C) DIC, (D) alkalinity, (E) pCO_2 and (F) pH to observations collected at seven stations in the Qatar EEZ in December 2018 and May 2019 (Izumi et al., 2022). For all comparisons, the model was sampled at the observation points.

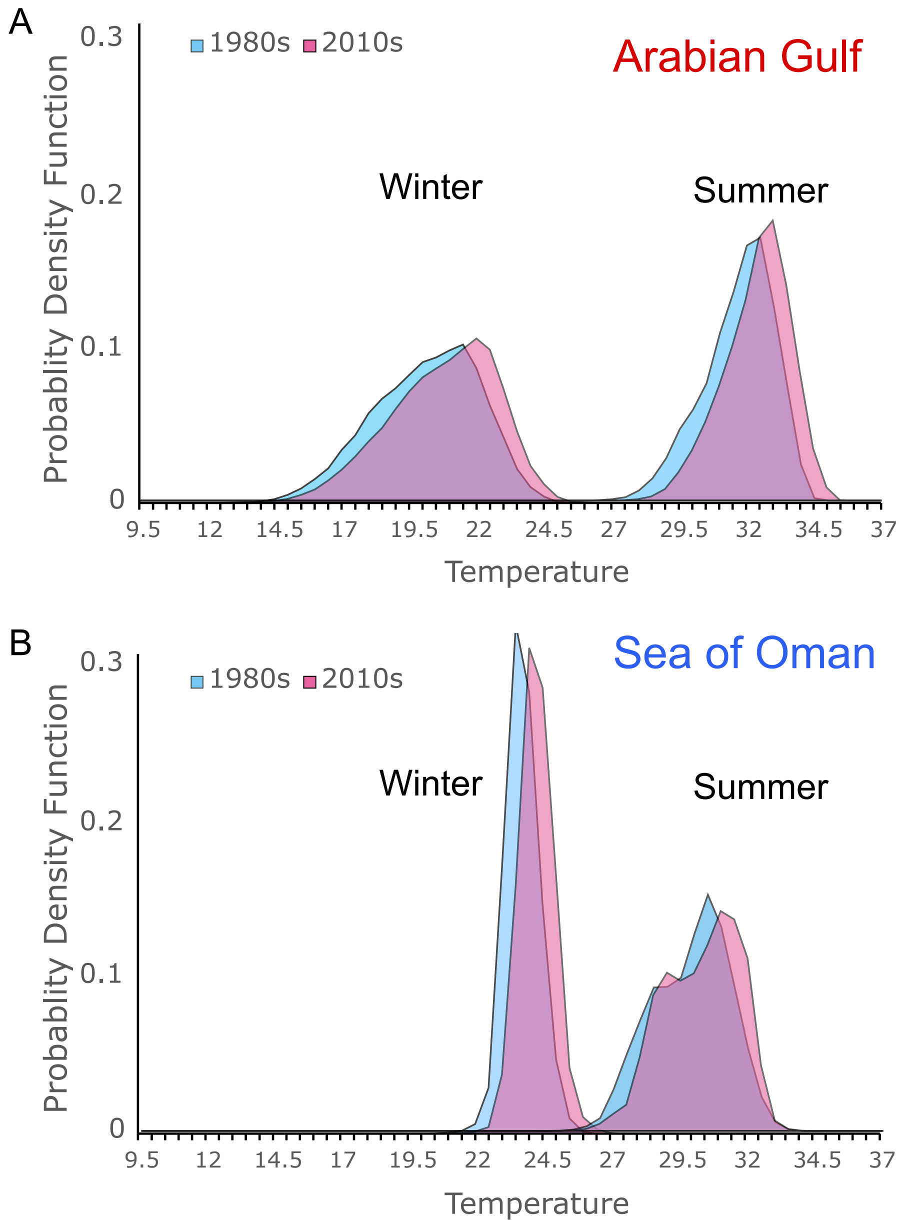

Figure S8. Change in temperature distributions in the AG and the SOO. Probability density function of simulated surface temperature during winter (JFM) and summer (JAS) in the 1980s (blue) and the 2010s (red) in the AG (top) and the SOO (bottom).

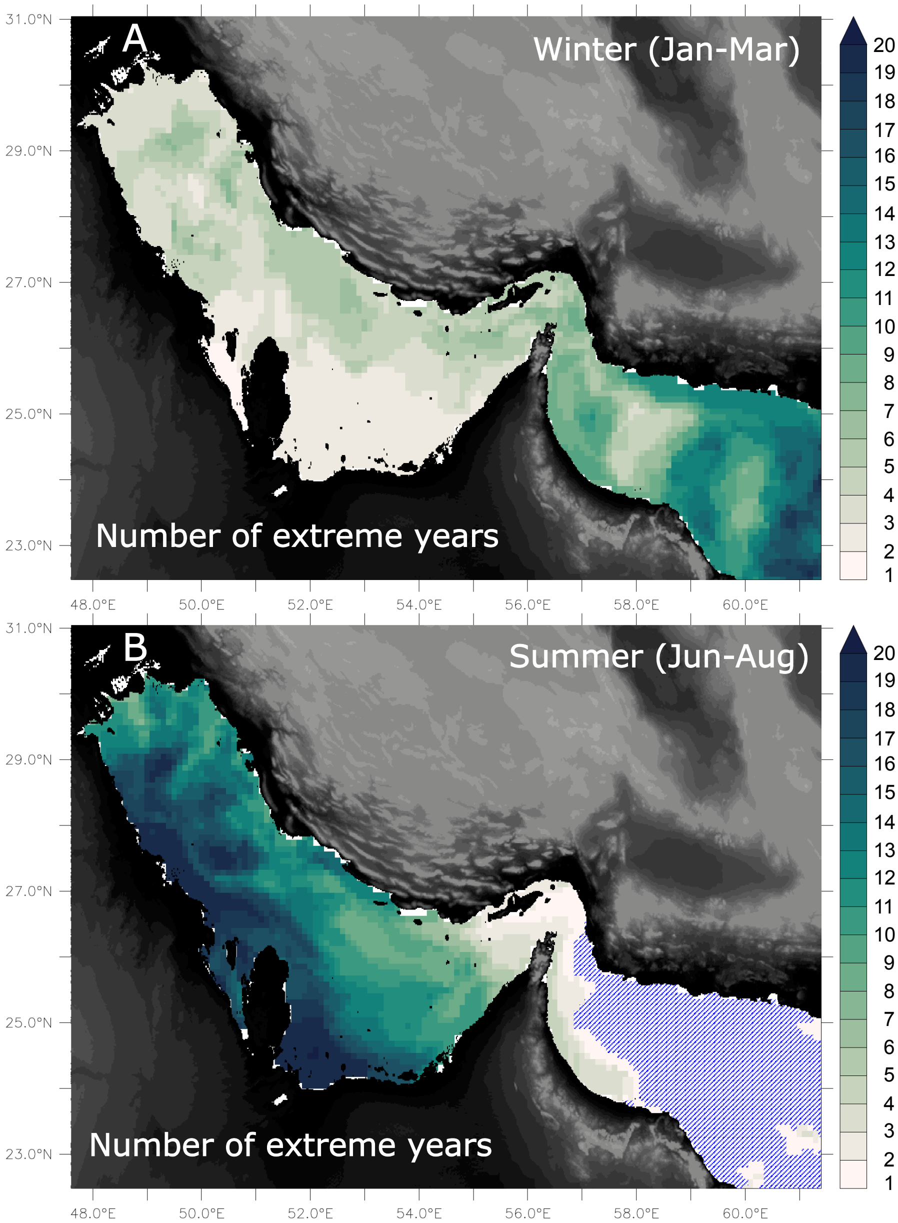

Figure S9. Number of extreme temperature years. Number of years where the average surface temperature for the season exceeds two standard deviations above the 1980s seasonal mean. (A) winter. (B) summer. Blue-hatching corresponds to areas where temperatures have not exceeded the defined threshold by the end of the study period.

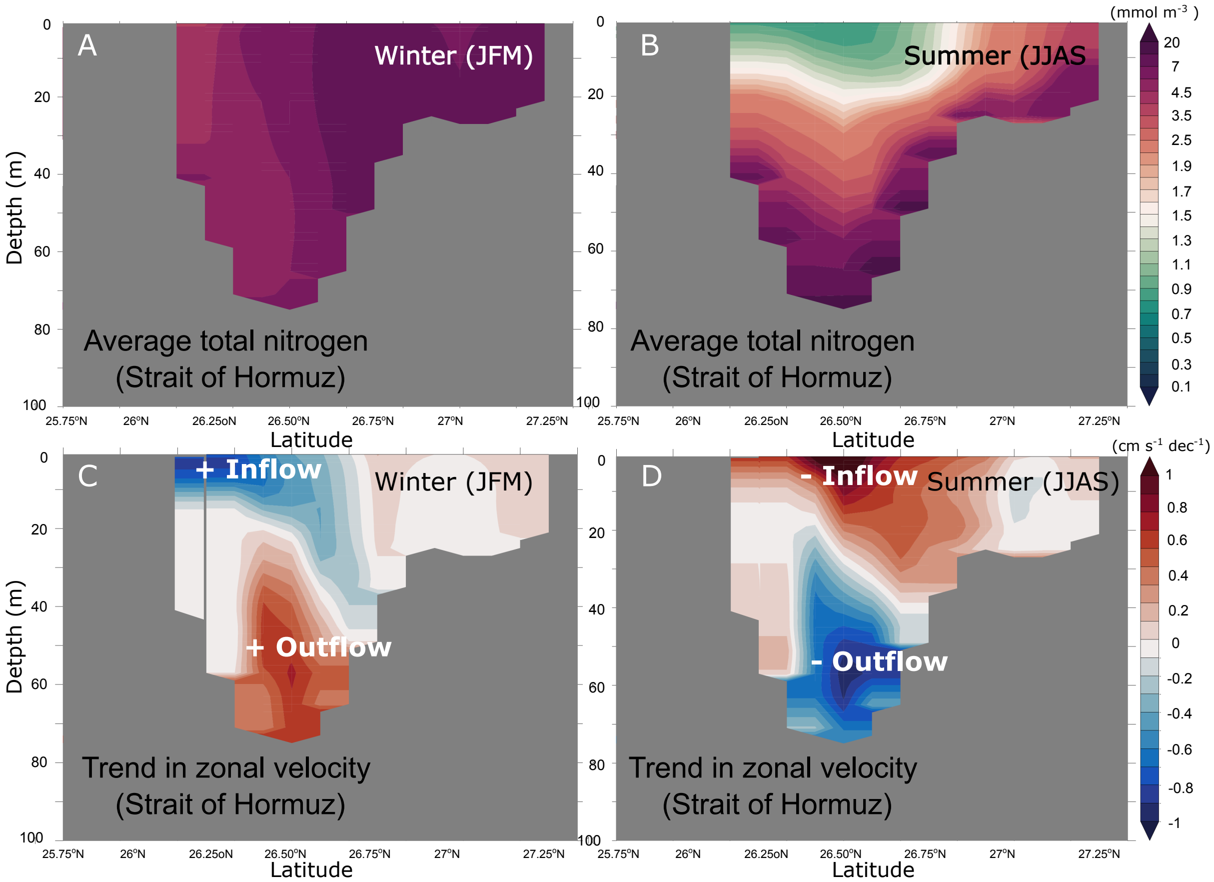

Figure S10. Nitrogen distribution and trends in zonal currents at the Strait. (A-B) vertical distribution of total nitrogen (in mmol m^{-3}) at Hormuz during winter (A) and summer (B). (C-D) Trends in zonal currents at Hormuz (in cm s^{-1} $decade^{-1}$) during winter (C) and summer (D). Positive values represent an increase of the Gulf outflow (or a decrease in the inflow).

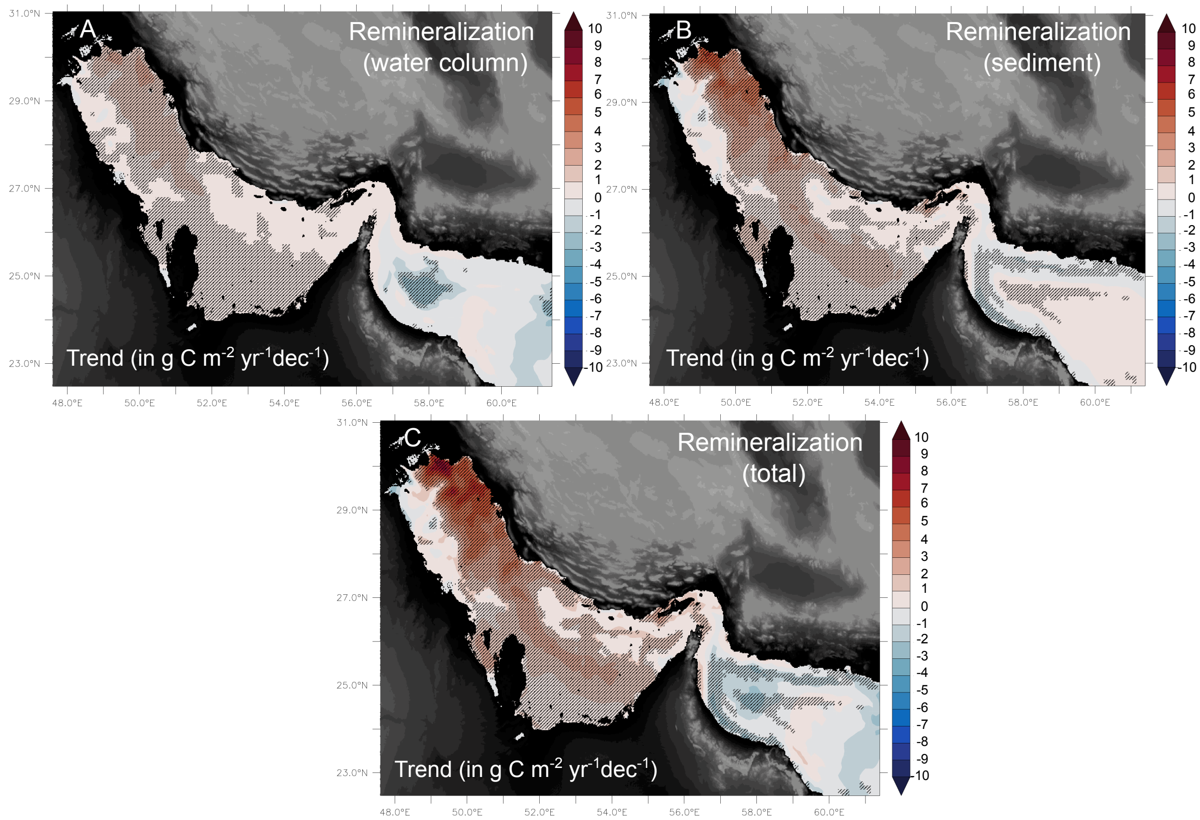

Figure S11. Changes in remineralization fluxes. Trends in remineralization fluxes (in g C m^{-2} yr^{-1} $decade^{-1}$) in the water-column (A), the sediment (B) and the total (water-column and sediment). Hatching indicates areas where trends are statistically significant at 95% confidence level.

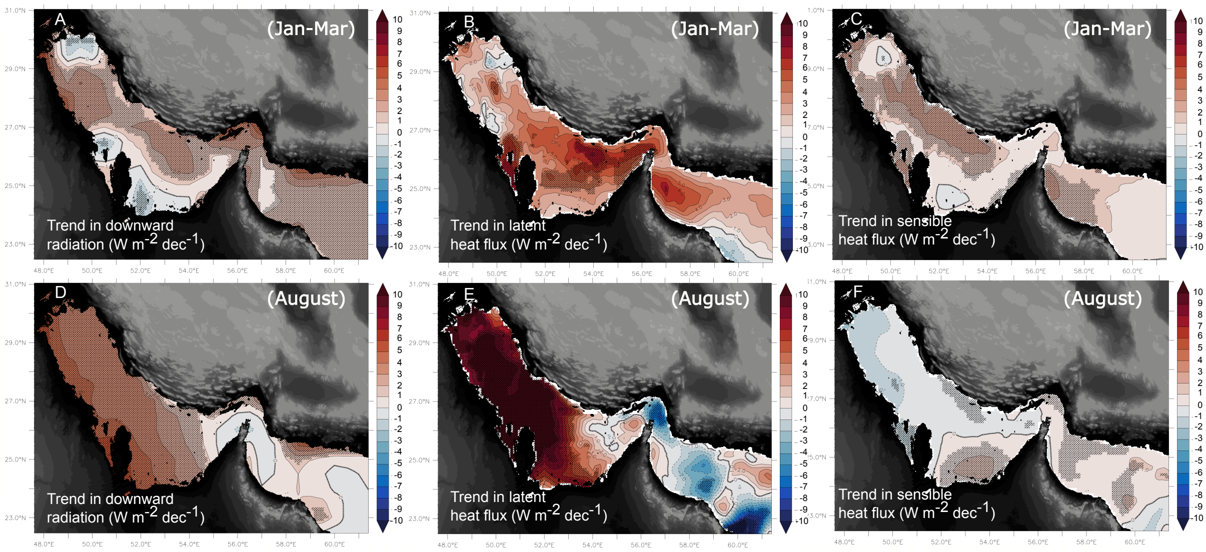

Figure S12. **Drivers of AG warming**. (A-C) Trends in downward radiation, latent and sensible heat fluxes (in W m^{-2} per decade) during winter months (JFM). (D-F) similar to (A-C) for the month of August. Hatching indicates areas where trends are statistically significant at 95% confidence level.

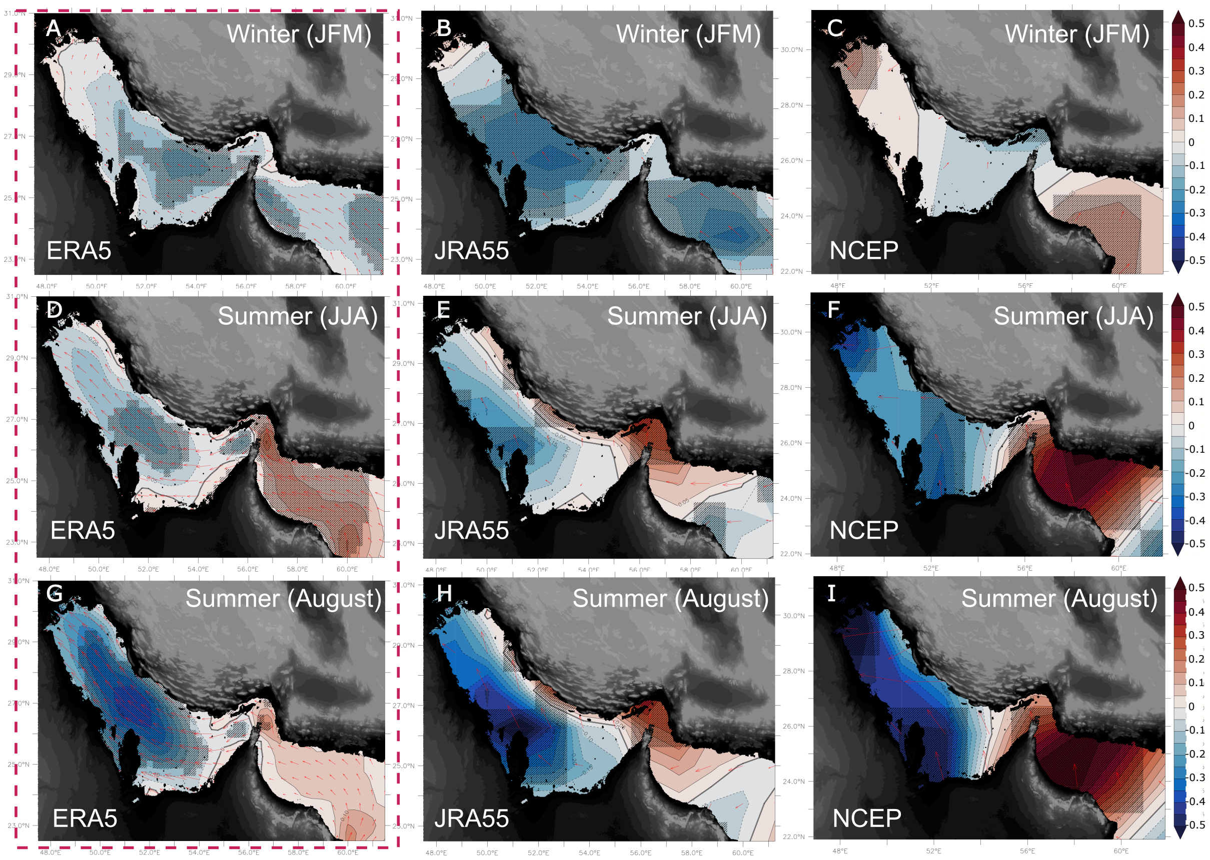

Figure S13. Changes in surface winds. Trends in surface winds in winter (A-C), summer (D-F) and for the month of August (G-I) based on ERA (left column), JRA55 (middle column) and NCEP (right column). Color shading indicates trends in wind speed (in m s^1 per decade), whereas arrows show trends in wind vector. Hatching indicates areas where trends are statistically significant at the 95% confidence level.

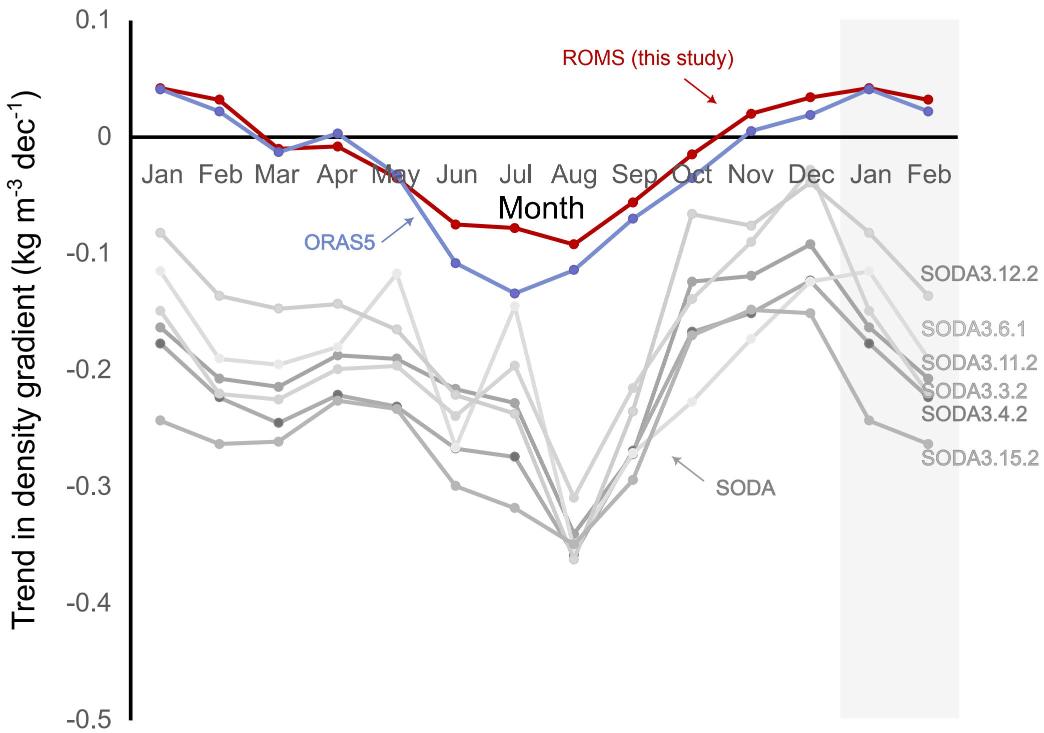

Figure S14. Changes in density gradient between the AG and the SOO based on different data products. Trends in density gradient between the AG and the SOO from ROMS (red), the ECMWF Ocean Reanalysis System 5 (ORAS5) reanalysis (blue) and different versions of Simple Ocean Data Assimilation (SODA) reanalyses (gray). The included SODA versions are: SODA3.3.2 (MERRA2), SODA3.4.2 (ERA-Interim), SODA3.6.1 (CORE2), SODA3.11.2 (DFS5.2), SODA3.12.2 (JRA55) and SODA3.15.2 (ERA5).

References

Ahmad, F., & Sultan, S. (1991). Annual mean surface heat fluxes in the arabian gulf and the net heat transport through the strait of hormuz. *Atmosphere-Ocean*, *29*(1), 54–61.

Al-Naimi, N., Raitsos, D. E., Ben-Hamadou, R., & Soliman, Y. (2017). Evaluation of satellite retrievals of chlorophyll-a in the arabian gulf. *Remote Sensing*, *9*(3), 301.

Al-Said, T., Naqvi, S., Al-Yamani, F., Goncharov, A., & Fernandes, L. (2018). Potential impact of human-induced physico-chemical changes in the arabian gulf on the oxygen minimum zone of the northwestern indian ocean. *Mar. Poll. Bull.*, *129*, 35–42.

Al-Yamani, F., & Naqvi, S. (2019). Chemical oceanography of the arabian gulf. *Deep Sea Research Part II: Topical Studies in Oceanography*, *161*, 72–80.

Behrenfeld, M. J., & Falkowski, P. G. (1997). Photosynthetic rates derived from satellite-based chlorophyll concentration. *Limnology and oceanography*, *42*(1), 1–20.

Chao, S.-Y., Kao, T. W., & Al-Hajri, K. R. (1992). A numerical investigation of circulation in the arabian gulf. *Journal of Geophysical Research: Oceans*, *97*(C7), 11219–11236.

de Verneil, A., Lachkar, Z., Smith, S., & Lévy, M. (2022). Evaluating the arabian sea as a regional source of atmospheric co 2: seasonal variability and drivers. *Biogeosciences*, *19*(3), 907–929.

Garcia, H., Boyer, T., Baranova, O., Locarnini, R., Mishonov, A., Grodsky, A. e., … others (2019). World ocean atlas 2018: Product documentation. *A. Mishonov, Technical Editor*.

Griffies, S. M., Danabasoglu, G., Durack, P. J., Adcroft, A. J., Balaji, V., Boning, C. W., … others (2016). Omip contribution to cmip6: experimental and diagnostic protocol for the physical component of the ocean model intercomparison project. *Geoscientific Model*

Development, 3231–3296.

Gruber, N., Clement, D., Carter, B. R., Feely, R. A., Van Heuven, S., Hoppema, M., ... others (2019). The oceanic sink for anthropogenic co2 from 1994 to 2007. *Science*, *363*(6432), 1193–1199.

Gruber, N., Frenzel, H., Doney, S. C., Marchesiello, P., McWilliams, J. C., Moisan, J. R., ... Stolzenbach, K. D. (2006). Eddy-resolving simulation of plankton ecosystem dynamics in the california current system. *Deep Sea Research Part I: Oceanographic Research Papers*, *53*(9), 1483–1516.

Izumi, C., Al-Thani, J. A., Yigiterhan, O., Al-Ansari, E. M. A., Vethamony, P., Sorino, C. F., ... Murray, J. W. (2022). Excess pco2 and carbonate system geochemistry in surface seawater of the exclusive economic zone of qatar (arabian gulf). *Marine Chemistry*, *247*, 104185.

Johns, W., Yao, F., Olson, D., Josey, S., Grist, J., & Smeed, D. (2003). Observations of seasonal exchange through the straits of hormuz and the inferred heat and freshwater budgets of the persian gulf. *Journal of Geophysical Research: Oceans*, *108*(C12).

Joos, F., & Spahni, R. (2008). Rates of change in natural and anthropogenic radiative forcing over the past 20,000 years. *Proceedings of the National Academy of Sciences*, *105*(5), 1425–1430.

Kämpf, J., & Sadrinasab, M. (2006). The circulation of the persian gulf: a numerical study. *Ocean Science*, *2*(1), 27–41.

Keeling, C. D., Piper, S. C., Bacastow, R. B., Wahlen, M., Whorf, T. P., Heimann, M., & Meijer, H. A. (2005). Atmospheric co2 and 13co2 exchange with the terrestrial biosphere and oceans from 1978 to 2000: observations and carbon cycle implications. In *A history of* *atmospheric co2 and its effects on plants, animals, and ecosystems* (pp. 83–113). Springer.

Key, R. M., Kozyr, A., Sabine, C. L., Lee, K., Wanninkhof, R., Bullister, J. L., ... Peng, T.-H. (2004). A global ocean carbon climatology: Results from global data analysis project (glodap). *Global biogeochemical cycles*, *18*(4).

Krishna, M., Prasad, M., Rao, D., Viswanadham, R., Sarma, V., & Reddy, N. (2016). Export of dissolved inorganic nutrients to the northern indian ocean from the indian monsoonal rivers during discharge period. *Geochimica et Cosmochimica Acta*, *172*, 430–443.

Lachkar, Z. (2014). Effects of upwelling increase on ocean acidification in the california and canary current systems. *Geophysical Research Letters*, *41*(1), 90–95.

Lachkar, Z., & Gruber, N. (2013). Response of biological production and air–sea co2 fluxes to upwelling intensification in the california and canary current systems. *Journal of Marine Systems*, *109*, 149–160.

Lachkar, Z., Mehari, M., Al Azhar, M., Lévy, M., & Smith, S. (2021). Fast local warming is the main driver of recent deoxygenation in the northern arabian sea. *Biogeosciences*, *18*(20), 5831–5849.

Lachkar, Z., Smith, S., Lévy, M., & Pauluis, O. (2016). Eddies reduce denitrification and compress habitats in the arabian sea. *Geophysical Research Letters*, *43*(17), 9148–9156.

Large, W. G., McWilliams, J. C., & Doney, S. C. (1994). Oceanic vertical mixing: A review and a model with a nonlocal boundary layer parameterization. *Reviews of Geophysics*, *32*(4), 363–403.

Lauvset, S. K., Key, R. M., Olsen, A., Van Heuven, S., Velo, A., Lin, X., ... others (2016). A new global interior ocean mapped climatology: The 1× 1 glodap version 2. *Earth System*

Science Data, *8*(2), 325–340.

Marchesiello, P., Debreu, L., & Couvelard, X. (2009). Spurious diapycnal mixing in terrain-following coordinate models: The problem and a solution. *Ocean Modelling*, *26*(3-4), 156–169.

Middelburg, J. J., Soetaert, K., Herman, P. M., & Heip, C. H. (1996). Denitrification in marine sediments: A model study. *Global Biogeochemical Cycles*, *10*(4), 661–673.

Olsen, A., Lange, N., Key, R. M., Tanhua, T., Álvarez, M., Becker, S., ... others (2019). Glodapv2. 2019–an update of glodapv2. *Earth System Science Data*, *11*(3), 1437–1461.

Orr, J. C., Fabry, V. J., Aumont, O., Bopp, L., Doney, S. C., Feely, R. A., ... others (2005). Anthropogenic ocean acidification over the twenty-first century and its impact on calcifying organisms. *Nature*, *437*(7059), 681–686.

Pous, S., Carton, X., & Lazure, P. (2004). Hydrology and circulation in the strait of hormuz and the gulf of oman—results from the gogp99 experiment: 1. strait of hormuz. *Journal of Geophysical Research: Oceans*, *109*(C12).

Quigg, A., Al-Ansi, M., Al Din, N. N., Wei, C.-L., Nunnally, C. C., Al-Ansari, I. S., ... others (2013). Phytoplankton along the coastal shelf of an oligotrophic hypersaline environment in a semi-enclosed marginal sea: Qatar (arabian gulf). *Continental Shelf Research*, *60*, 1–16.

Ramesh, R., Purvaja, G., & Subramanian, V. (1995). Carbon and phosphorus transport by the major indian rivers. *Journal of Biogeography*, 409–415.

Saleh, A., Abtahi, B., Mirzaei, N., Chen, C.-T. A., Ershadifar, H., Ghaemi, M., ... Abedi, E. (2021). Hypoxia in the persian gulf and the strait of hormuz. *Marine Pollution Bulletin*, *167*, 112354.

Shchepetkin, A. F., & McWilliams, J. C. (2005). The regional oceanic modeling system (roms): a split-explicit, free-surface, topography-following-coordinate oceanic model. *Ocean modelling*, *9*(4), 347–404.

Wanninkhof, R. (1992). Relationship between wind speed and gas exchange over the ocean. *Journal of Geophysical Research: Oceans*, *97*(C5), 7373–7382.

Yao, F., & Johns, W. E. (2010). A hycom modeling study of the persian gulf: 2. formation and export of persian gulf water. *Journal of Geophysical Research: Oceans*, *115*(C11).

Zuo, H., Balmaseda, M. A., Tietsche, S., Mogensen, K., & Mayer, M. (2019). The ecmwf operational ensemble reanalysis–analysis system for ocean and sea ice: a description of the system and assessment. *Ocean science*, *15*(3), 779–808.